







DUDLEY KNOX LIBRARY  
NAVAL POSTGRADUATE SCHOOL  
MONTEREY, CALIFORNIA 93943



# NAVAL POSTGRADUATE SCHOOL

## Monterey, California



# THESIS

A MODEL STUDY OF THE EQUATORIAL  
OCEAN SURFACE TEMPERATURE RESPONSE  
TO WIND FORCING DURING EL NINO

by

Jeroen J. Waterreus

June 1985

Thesis Advisor:

R. L. Haney

Approved for public release, distribution unlimited

T227308



REPORT DOCUMENTATION PAGE		READ INSTRUCTIONS BEFORE COMPLETING FORM
1. REPORT NUMBER	2. GOVT ACCESSION NO.	3. RECIPIENT'S CATALOG NUMBER
4. TITLE (and Subtitle) A Model Study of the Equatorial Ocean Surface Temperature Response to Wind Forcing During El Nino		5. TYPE OF REPORT & PERIOD COVERED Master's Thesis June 1985
7. AUTHOR(s) Jeroen J. Waterreus		6. PERFORMING ORG. REPORT NUMBER
9. PERFORMING ORGANIZATION NAME AND ADDRESS Naval Postgraduate School Monterey, CA 93943-5100		8. CONTRACT OR GRANT NUMBER(s)
11. CONTROLLING OFFICE NAME AND ADDRESS Naval Postgraduate School Monterey, CA 93943-5100		10. PROGRAM ELEMENT, PROJECT, TASK AREA & WORK UNIT NUMBERS
14. MONITORING AGENCY NAME & ADDRESS (if different from Controlling Office)		12. REPORT DATE June 1985
		13. NUMBER OF PAGES 67
		15. SECURITY CLASS. (of this report)
		15a. DECLASSIFICATION/DOWNGRADING SCHEDULE
16. DISTRIBUTION STATEMENT (of this Report) Approved for public release; distribution unlimited		
17. DISTRIBUTION STATEMENT (of the abstract entered in Block 20, if different from Report)		
18. SUPPLEMENTARY NOTES		
19. KEY WORDS (Continue on reverse side if necessary and identify by block number) El Nino, horizontal advection, sea surface temperature anomaly, anomalous entrainment heat flux, Kelvin wave speed, coupled atmosphere-ocean model, mixed layer physics, atmosphere feedbacks, southern oscillation		
20. ABSTRACT (Continue on reverse side if necessary and identify by block number) The purpose of this research is to investigate specific processes that contribute to large scale equatorial SST variability, and by comparison with observation, verify the realism of the model's thermal response to prescribed forcing in the atmosphere. Building on previous work, more realistic thermodynamic processes are incorporated in the ocean part of Rennick's (1985) coupled ocean-atmosphere model and an examination of its response to prescribed wind forcing is conducted.		

The dynamic ocean model is based on the shallow water momentum equations forced by a surface wind stress. It is linearized about a motionless state with a zonally sloping pycnocline depth which is in balance with the surface stress caused by the zonal wind of the atmospheric basic state. This study investigates the effect of turbulent vertical mixing of heat, in contrast to horizontal advection, for the generation of SST anomalies in the equatorial region of the Pacific. Results showed that the SST anomaly produced by turbulent mixing was two orders of magnitude smaller than, and 90 degrees out of phase with, the SST anomaly generated by horizontal advection.

Although the small magnitude of the anomalous entrainment heat flux would seem to justify its neglect, the phase difference raises the question of whether it would be significant in a coupled ocean-atmosphere system. Therefore, two cases of the coupled model were designed to investigate if the different SST responses caused by turbulent mixing and by horizontal advection would cause growth of a coupled disturbance. The results were that neither ocean process causes growth.



Approved for public release; distribution is unlimited.

A Model Study of the Equatorial  
Ocean Surface Temperature Response  
to Wind Forcing During El Nino

by

Jeroen J. Waterreus  
Lieutenant, United States Navy  
B.S., United States Naval Academy, 1977

Submitted in partial fulfillment of the  
requirements for the degree of

MASTER OF SCIENCE IN METEOROLOGY AND OCEANOGRAPHY

from the

NAVAL POSTGRADUATE SCHOOL  
June 1985

THESIS  
W22987  
C.1

## ABSTRACT

The purpose of this research is to investigate specific processes that contribute to large scale equatorial SST variability, and by comparison with observation, verify the realism of the model's thermal response to prescribed forcing in the atmosphere. Building on previous work, more realistic thermodynamic processes are incorporated in the ocean part of Rennick's (1985) coupled ocean-atmosphere model and an examination of its response to prescribed wind forcing is conducted.

The dynamic ocean model is based on the shallow water momentum equations forced by a surface wind stress. It is linearized about a motionless state with a zonally sloping pycnocline depth which is in balance with the surface stress caused by the zonal wind of the atmospheric basic state. This study investigates the effect of turbulent vertical mixing of heat, in contrast to horizontal advection, for the generation of SST anomalies in the equatorial region of the Pacific. Results showed that the SST anomaly produced by turbulent mixing was two orders of magnitude smaller than, and 90 degrees out of phase with, the SST anomaly generated by horizontal advection.

Although the small magnitude of the anomalous entrainment heat flux would seem to justify its neglect, the phase difference raises the question of whether it would be significant in a coupled ocean-atmosphere system. Therefore, two cases of the coupled model were designed to investigate if the different SST responses caused by turbulent mixing and by horizontal advection would cause growth of a coupled disturbance. The results were that neither ocean process causes growth.

## TABLE OF CONTENTS

I.	INTRODUCTION . . . . .	9
A.	BACKGROUND . . . . .	9
B.	THE PROBLEM . . . . .	11
II.	THEORIES/MODELS . . . . .	14
A.	INITIAL COUPLED AIR-SEA MODEL USED BY RENNICK (1985) . . . . .	14
B.	INCLUSION OF WIND STRESS ANOMALY FORCING . . .	16
C.	INCLUSION OF OCEAN MIXING MODEL . . . . .	18
III.	RESULTS AND OBSERVATIONS . . . . .	25
A.	EFFECTS OF HORIZONTAL ADVECTION ONLY (CASE ONE) . . . . .	25
B.	EFFECTS OF MIXING ONLY (CASE TWO) . . . . .	28
C.	HORIZONTAL ADVECTION PLUS MIXING (CASE THREE) . . . . .	30
D.	COUPLED MODE WITH HORIZONTAL ADVECTION OF SST (CASE FOUR) . . . . .	30
E.	COUPLED MODE WITH TURBULENT MIXING ONLY (CASE FIVE) . . . . .	31
IV.	CONCLUSIONS . . . . .	33
	LIST OF REFERENCES . . . . .	63
	INITIAL DISTRIBUTION LIST . . . . .	66



## LIST OF FIGURES

4.1	Anamolous winds for June, July, August 1982 Observed (upper) and computer generated(lower); contours 5m/sec(upper) and .2m/sec(lower) . . . . .	34
4.2	Anamolous winds for September, October, November 1982, observed(upper) and computer generated (lower); contours 5m/sec( upper) and .2m/sec(lower) . . . . .	35
4.3	Anamolous winds for December, January, February 1982-1983, observed(upper) and computer generated (lower); contours 5m/sec(upper) and .2m/sec(lower) . . . . .	36
4.4	Anamolous winds for March, April, May 1983, observed(upper) and computer generated (lower); contours 5m/sec(upper) and .2m/sec(lower) . . . . .	37
4.5	Anamolous winds for June, July, August 1983, observed(upper) and computer generated(lower); contours 5m/sec(upper) and .2m/sec(lower) . . . . .	38
4.6	Case one, zonal wind anomaly (m/sec) time-longitude plot . . . . .	39
4.7	Case one, depth (m) and current anomalies (m/sec) for entire basin (day 50 and 100) . . . . .	40
4.8	Case one, depth (m) and current anomalies (m/sec) for entire basin (day 150 and 200) . . . . .	41
4.9	Case one, depth (m) and current anomalies (m/sec) for entire basin (day 250 and 300) . . . . .	42
4.10	Case one, depth (m) and current anomalies (m/sec) for entire basin (day 350 and 400) . . . . .	43
4.11	Case one, depth (m) and current anomalies (m/sec) for entire basin (day 450 and 500) . . . . .	44

4.12	Case one, SST anomalies (deg C) for entire basin (day 50 and 100) . . . . .	45
4.13	Case one, SST anomalies (deg C) for entire basin (day 150 and 200) . . . . .	46
4.14	Case one, SST anomalies (deg C) for entire basin (day 250 and 300) . . . . .	47
4.15	Case one, SST anomalies (deg C) for entire basin (day 350 and 400) . . . . .	48
4.16	Case one, SST anomalies (deg C) for entire basin (day 450 and 500) . . . . .	49
4.17	Case one, pycnocline depth anomaly (m) time-longitude plot . . . . .	50
4.18	Case one, SST anomaly (deg C) time-longitude plot . . . . .	51
4.19	Case two, SST anomalies (deg C) for entire basin (day 50 and 100) . . . . .	52
4.20	Case two, SST anomalies (deg C) for entire basin (day 150 and 200) . . . . .	53
4.21	Case two, SST anomalies (deg C) for entire basin (day 250 and 300) . . . . .	54
4.22	Case two, SST anomalies (deg C) for entire basin (day 350 and 400) . . . . .	55
4.23	Case two, SST anomalies (deg C) for entire basin (day 450 and 500) . . . . .	56
4.24	Case two, SST anomaly (deg C) time-longitude plot . . . . .	57
4.25	Case two, pycnocline depth anomaly (m) time-longitude plot . . . . .	58
4.26	Case four, pycnocline depth anomaly (m) time-longitude plot . . . . .	59
4.27	Case four, SST anomaly (deg C) time-longitude plot . . . . .	60
4.28	Case five, pycnocline depth anomaly (m) time-longitude plot . . . . .	61

4.29	Case five, SST anomaly (deg C) time-longitude	
	plot . . . . .	62



## I. INTRODUCTION

### A. BACKGROUND

The El Nino/Southern Oscillation (ENSO) is the dominant global climate signal on time scales of a few months to a few years (Rassmusson, 1984). ENSO's have appeared every few years for centuries, and there have been at least six since 1951.

The aspect of an ENSO event is that once it starts, it evolves rather predictably for as long as 18 months. The meteorology of a typical ENSO event can be described in terms of the spatial evolution and the time of occurrence relative to the seasonal cycle, which are strikingly similar for most ENSO events (Rassmusson, 1984). The year prior to the event is characterized by a strong trough over the Maritime Continent (Australian, Indonesian, Southern Asia Monsoon regions) and a strong south Pacific ocean High. This pressure gradient is called the Southern Oscillation Index (SOI) and is defined as the difference in surface pressure between Tahiti and Darwin. A slackening of the pressure gradient (SOI) at the end of the first year, along with a weakening of the easterlies, causes positive sea-surface temperature anomalies (SSTA'S) to propagate eastward across the equatorial Pacific Ocean to the coast of Chile by one or more of the following possible dynamic mechanisms (Philander, 1983b):

- (1) anomalous southward flow of warm water due to the slackening of southeast trades;
- (2) changes in large-scale equatorial zonal currents associated with local changes in the curl of the wind stress; and

- (3) local and remote warming due to weakening of equatorial easterlies.

The ENSO year is characterized by rapid positive and negative surface pressure changes at Darwin and Tahiti and sea-surface temperature increases near the Peru coast. Also of crucial importance is the major eastward shift of the Maritime Continent convection region. In the upper troposphere, an anticyclonic couplet straddles the region of enhanced rainfall in the Central Equatorial Pacific, causing a stronger-than-normal eastern North Pacific jet with persistent upper-troposphere easterlies. At the onset of El Nino, the Southern Hemisphere experiences anomalies in large scale flow in the formation of a huge anticyclone at 15 degrees south. Northward and eastward of the anticyclonic center is an apparent wave train of positive and negative anomaly centers which lies along a great circle and may reflect a Rossby wave train (Wright, 1977). In the western North Pacific ocean, low-level westerlies extend eastward during the ENSO event and create an environment of low level cyclonic relative vorticity near the dateline.

Scientists thought they had a reliable picture of how an ENSO event started and developed, but then the 1982-1983 ENSO event occurred. Even though in scientific terms it came along at the expected time, it did not occur in the expected manner. The warm water typical of ENSO usually first appears off the coast of South America early in the year and then gradually spreads westward. Instead, the warming in 1982 began in May in the central Pacific and gradually spread eastward. By strict definition this was not an ENSO event, but it turned out to be the strongest ENSO event in nearly a century.

The 1982-1983 ENSO event is being intensely studied, because it was the most intensely measured event. It was found that the sea-surface temperature (SST) vice SSTa were

closely related to the anomalous convective activity. The eastward migration of the region of maximum SST was accompanied by an abnormally large heat loss to the atmosphere, and a westerly wind anomaly over and to the west of the SST maximum. The combined system of warm SST, convection and westerly wind anomalies then progressed steadily to the east. This ENSO event had two sequential but interrelated events (Rasmusson, 1984). The first event was the initial warming near the eastern boundary associated with the weakening of the eastern South Pacific ocean anticyclone, and the second was the broad scale warming of the equatorial Pacific from near the date line eastward.

## B. THE PROBLEM

Numerical models based on the shallow water equations have been very useful in investigating and studying ENSO events. Hurlburt et al. (1976) and McCreary (1976) investigated ENSO-like events by forcing their simple models with abrupt reductions in surface wind stress. Busalacchi and O'Brien (1981) and Busalacchi et al. (1983) successfully simulated the observed variability of sea level for a period 1961-1978 using a shallow water equation ocean model with a prescribed surface wind stress based on monthly mean averages. The response of the tropical atmosphere to anomalous equatorial heat sources using the shallow water equations was studied by Gill, (1980). Gill and Rasmusson (1983) used a heat source based on the observed mean of outgoing long wave radiation from June 1982 to January 1983 and found there was an agreement between their model wind and the corresponding observed wind field anomalies.

The degree of interaction between the simultaneously evolving atmospheric and oceanic elements of ENSO events has been explored in a limited sense by Lau (1981) and by



McCreary (1983). In their models the atmosphere assumes one of two prescribed states dependent upon the distribution of the model-determined pycnocline depth anomaly. The coupled model produced an oscillation between ENSO (warm ocean) and a normal (cold) ocean.

The coupled air-ocean models were designed to answer critical questions concerning the initiation of an ENSO event. The questions involve the mechanisms that are responsible for ENSO, the timing of the event relative to the annual cycle, the time interval between events, and the eastward migration of the event. Rennick (1985) utilized a simple numerical model which allowed interactive coupling between the atmosphere and the equatorial ocean. An investigation was made to determine the extent to which eastward extension of the warm water pool in the western Pacific during ENSO could be attributed to the atmospheric circulation induced by the warm water itself. These models ignored vertical mixing and attempted to isolate the role of horizontal advection of temperature. The result of this numerical experimentation was that the atmospheric circulation due to an anomalously warm western Pacific did not induce a self perpetuating eastward migration of warm water and anomalous convection.

The present problem involves using the same dynamic models used by other investigators (ie. McCreary, 1976, 1983; Busalacchi and O'Brien, 1981; Bussalacchi et al., 1983; Lau, 1981; Rennick, 1985). Rennick and Haney (1985), using a linear coupled atmosphere-ocean model, found that the analytic solutions are very sensitive to whether heating in the atmosphere is parameterized in terms of the oceanic pycnocline depth anomaly (Philander et al., 1983) or in terms of the advectively determined sea surface-temperature anomaly (Rennick and Haney 1985, Rennick 1985). The objective of this research is to investigate what determines sea

surface-temperature variability using the ocean model part of the coupled atmosphere and equatorial ocean model of Rennick (1985). This will be done by incorporating more ocean thermodynamics than previously considered.

## II. THEORIES/MODELS

### A. INITIAL COUPLED AIR-SEA MODEL USED BY RENNICK (1985)

The numerical model used here is a coupled model in which the atmosphere and ocean are each represented by the shallow water equations. The model will be used primarily in the ocean-only mode, and, therefore, all theory pertinent to the ocean will be discussed in detail.

The equations for the ocean are solved in an equatorial basin having 120 degrees longitude by 30 degrees latitude centered on the equator at 140 degrees west longitude. The ocean is forced by a surface wind stress where the mean wind is easterly at five meters per second, and an anomalous westerly wind patch (Guassian) is utilized to depict the anomalous conditions experienced during ENSO.

Two important features are included in this model which are absent in earlier work. First, the annually averaged pycnocline depth is set at two hundred meters in the west and eighty meters in the east. This zonally sloping pycnocline depth is in balance with the surface stress attributable to the mean zonal wind. This modification allows the pycnocline anomalies computed by the model, especially in the eastern part of the basin, to be smaller than those associated with a uniform mean pycnocline depth.

Secondly, rudimentary mixed layer physics is included along with the dynamic processes of the shallow water equations. This allows the the sea-surface temperature to be computed directly. This is very important in an interactive system, as pointed out by Hanson (1983), and Rennick and Haney (1985).

The model equations for the ocean are then written as

$$(1) \quad du/dt - fv + g' dh/dx = Fx + K \nabla^2 u$$



$$(2) \quad dv/dt + fu + g' dh/dy = Fy + K \nabla^2 v$$

$$(3) \quad dh/dt + \nabla \cdot (Hv) = 0$$

$$(4) \quad dT/dt + \nabla \cdot \bar{T} = -XT$$

$H(x)$  is the pycnocline depth of the motionless ocean basic state,  $\bar{T}$  is the mean sea-surface temperature, and  $g'$  is the reduced gravity for the two layer ocean. There is no mean flow in the ocean.  $F_x$  and  $F_y$  are the respective wind stress in the eastward and northward directions. The ocean thermodynamic equation (4) includes horizontal advection by the dynamically produced currents and a surface heat loss term,  $XT$ . Based upon arguments of Schopf (1983), the time scale for the surface heat loss ( $1/X$ ) is chosen to be about one year. In this initial model, effects of vertical mixing in the ocean were ignored in order to isolate the role of horizontal advection.

The model's basic state is defined by solid (constant angular velocity) eastern rotation in the atmosphere ( $U=-5\text{m/s}$ ), the slanting pycnocline, and the mean sea-surface temperature  $\bar{T}$  decreasing linearly from  $30^\circ\text{C}$  at the western ocean boundary to  $25^\circ\text{C}$  at the eastern boundary. In order to define the initial (anomalous) conditions for the ocean model, a sea-surface temperature anomaly was first imposed at the western edge of the ocean. This sea-surface temperature anomaly was held fixed while the atmosphere was spun up from its basic state (zero anomaly) to one of approximate equilibrium with the heating anomaly associated with the imposed sea-surface temperature distribution. The resulting zonal wind anomaly was used to compute an approximately balanced mixed layer depth anomaly. This mixed layer depth anomaly together with the original SST anomaly constitute the oceanic initial conditions. The currents were initially zero. The wind forcing was the total (solid rotation plus

anomaly) wind after spinup. In the ocean-only mode the atmospheric surface wind field is held fixed, and the ocean is allowed to evolve from its initial state in response to the fixed surface stress. Since the surface wind field was held fixed, there is no feedback due to changes in sea surface-temperature.

The ocean's response to these conditions (Rennick, 1985) was an eastward propagating Kelvin wave whose currents produced warm advection along most of the equator. When the Kelvin wave reached the eastern boundary (80 degrees west longitude), some of its energy reflected westward as a Rossby wave. As this Rossby wave migrated westward, it caused the sea-surface temperature tendency to reverse, thereby defining the peak of the warm event in the model ocean. Most important, however, is the fact that the resulting SST anomaly was quite weak. These results point out the need for further study, including the possible need to include ocean to atmosphere feedbacks, and additional physical processes such as vertical mixing and radiation in the determination of the sea-surface temperature. These results provided motivation for the present thesis.

## B. INCLUSION OF WIND STRESS ANOMALY FORCING

The additional oceanic physical processes were tested in the ocean-only version of the model forced by a prescribed, but moving, wind stress anomaly field characteristic of an ENSO event. The wind patch used to better describe the ENSO wind field was suggested by Blundell and Gill (1983).

A simple analytical form was chosen to model the observed stress data. The form of the equation denoting the eastward component of stress ( $F_x$ ) is

$$(5) \quad F_x = F(t) \cdot G(KSI) \cdot H(y)$$

$F(t)$  is the time envelope for a forcing of constant shape, propagating with constant speed in the X-direction. The wind stress (Figures 4.1-4.6) lasts for fifteen months, with a sinusoidal rise and fall.

$G(KSI)$  is the wind forcing patch and covers sixty degrees of longitude.  $G(KSI)$  is given by

$$(6) \quad G(KSI) = \cos(3 \cdot KSI) \text{ for } |KSI| < \pi/6$$

$$(7) \quad G(KSI) = 0 \text{ for } |KSI| > \pi/6$$

where KSI is expressed in radians for the computer model and is given by

$$(8) \quad KSI = X - ct.$$

Here X is longitude (radians) measured eastward from the western boundary, t is time and c is chosen to be a motion of 90 degrees longitude in 11 months (Rennick, 1985).

The north/south extent of the wind patch is described by the function  $H(y)$ , where y is latitude (radians), and

$$(9) \quad H(y) = (1 - \theta^2) \exp(-3 \cdot \theta^2/4)$$

$$(10) \quad \theta = ay$$

The value of (a) is 5.73, in order for  $H(y)$  to have a zero crossing at 10 degrees latitude. In the model, if  $H(y)$  in equation (9) is less than zero, then  $H(y)$  is set equal to zero. This was done because values dropped off very quickly, and an easterly wind forcing over any part of the ocean domain was undesirable.

Figures 4.1-4.5 show a comparison of the observed anomalous wind fields for 850 mb from the 1982-1983 El Nino/Southern Oscillation Quick Look Atlas (1983) with those of the computer generated anomalous wind fields at comparable times (lower panel). The lower panel encompasses an area from  $15^\circ$  north to  $15^\circ$  south latitude and  $130^\circ$  east to

50° west longitude. The central longitude is at 140° west vice 180° longitude (upper panels ) and therefore a box has been included in the upper panels showing the basin boundaries of the model. The magnitude of the wind fields differ because of the parameters selected for the model, but the direction of the winds and the movement of the patch correspond very well with the observed field. Figure 4.6 is a time-longitude plot of the computer generated anomalous surface zonal wind at the equator and shows its eastward movement, magnitude and location for five hundred days. Divergence and convergence patterns can be inferred from Figure 4.6 in that convergence will occur ahead of the wind patch and divergence will occur behind.

### C. INCLUSION OF OCEAN MIXING MODEL

To investigate specific processes that contribute to large scale equatorial SST variability, an integration of the temperature equation is integrated over depth. Assuming that non-linear terms are negligible, the equation has the form:

$$(11) \quad dT'/dt = -\bar{V} \cdot \nabla T' - V' \cdot \nabla \bar{T} - H'/\bar{H} \{ (\overline{WT})_0 - (\overline{WT})_{-H} \} - (\overline{WT})'_0/\bar{H} + (\overline{WT})'_{-H}/\bar{H}$$

The overbar represents a mean value and the prime represents an anomaly. The term  $(\overline{WT})'$  represents the turbulent vertical heat flux, with  $\overline{WT}$  the climatological value. The subscript 0 refers to the sea-surface and -H to the base of the mixed layer. The first term is the change of anomalous temperature with time. The second term represents the horizontal advection of the SST anomaly by the mean current and on the basis of available data (Niiler, 1982; Weare, et.al., 1981; Wyrski, 1981) can be considered negligible. The third term is the horizontal advection of the mean SST by the



anomalous current. This is the term Gill (1983) and Harrison and Schopf (1984) found to dominate the SST anomaly development during the early phases of ENSO. Term three is the only term which has been utilized in Rennick's (1985) studies.

Present estimates suggest that some of the other terms may become significant as a warm anomaly moves eastward into a region where the pycnocline depth is smaller. One of these terms is term four of equation (11). This is a SST anomaly generating term, where anomalous warming or cooling occurs by converging the normal amount of heat into an anomalously thin ( $H' < 0$ ) or thick ( $H' > 0$ ) layer. Term five of equation (11) is the anomalous surface heat flux and includes all components of heating such as sensible, latent, and solar heating. It is term six, which is the anomalous entrainment heat flux, that will be of most interest in this thesis.

Conducting a rough estimate of the scale of all the terms, it can be shown that no term is larger than the anomalous entrainment heat flux term, except possibly the term which is already included in the model. The horizontal advection of mean SST by the anomalous current is the most important, but it is believed that the contribution of the anomalous entrainment heat flux is perhaps comparable. Therefore, equation (11) will be simplified as follows:

$$(12) \quad dT'/dt = -U' \cdot dT/dx + (WT)'_{-H} / \bar{H}$$

This equation states that the change of anomalous temperature with time is equal to the horizontal advection of the mean SST by an anomalous east-west current plus the anomalous entrainment heat flux divided by the mean pycnocline depth.

To close the ocean model it is necessary to include a consistent mass flux when entrainment heat flux is present.

Integrating the continuity equation for an incompressible fluid gives

$$(13) \quad dH'/dt = -\nabla \cdot (\hat{V}\bar{H}) = We'$$

$H'$  is the anomalous pycnocline depth,  $\bar{H}$  is the mean pycnocline depth, and  $\hat{H}\bar{V}$  is expressed as

$$(14) \quad \hat{H}\bar{V} = \int_{-H}^0 V' dz$$

$We'$  is the anomalous entrainment mixing and is expressed in terms of the entrainment heat flux as

$$(15) \quad We' = -(WT)_{-H}' / \Delta T$$

$\Delta T$  is the temperature jump at the base of the layer and is prescribed as 3° C in the model (Wyrтки, 1981).

In order to obtain the anomalous heat flux at the base of the layer a modified version of the Kraus and Turner (1967) bulk closure model of the upper ocean will be used. In this model,

$$(16) \quad (WT)_{-H} = -\Lambda \{ (((1+K) \cdot m \cdot (WSTAR**3)) / (ALPHA \cdot g \cdot H)) + (WT)_0 - (1-K) \cdot \Lambda \cdot \{ (WT)_0 \} - S(F,H) \}$$

The left hand side is the total (mean plus anomalous) entrainment heat flux. It is necessary to subtract the mean entrainment heat flux to get the anomalous entrainment heat flux.  $\Lambda$  is the heavy side function.  $WSTAR$  is the friction velocity in the water due to the surface wind stress,  $ALPHA$  is the thermal expansion coefficient for sea water, and  $g$  is gravity.

The coefficient  $K \sim 0.2$  (Stage and Businger, 1981) accounts for dissipation of turbulence produced by shear and convection in the upper ocean, while the coefficient  $m \sim 2.0$  (Niiler and Kraus, 1977) accounts for the fact that the production of turbulence by stress driven shear in the upper ocean is only proportional to  $(WSTAR**3)/(ALPHA \cdot g \cdot H)$

(see Niiler and Kraus, 1977).  $S(F,H)$  is the stabilizing effect of solar radiation where

$$(17) \quad S(F,H) = 2 \cdot \{ .5 \cdot (F_0 - F_{-H}) - (1./\bar{H}) \cdot \int_{-H}^0 F(z) dz \}$$

$F(z)$  is the downward flux of solar radiation. It is exponential in form, and it is a maximum at the surface and minimum at greater depth. Since  $F(z)$  is not linear in  $z$ , but rather exponential, its effect is to stably stratify the mixed layer, and this requires energy from the wind and convective mixing in order to mix the temperature to an isothermal state.

Equations (16) and (17) are used to obtain the solution for the anomalous heat flux. The anomalous form is derived under several assumptions. The climatological state is assumed such that  $(WT)_0 > 0$  and  $(WT)_{-H} < 0$ . Also, in the general state  $(WT)_0 > 0$ . Thus, the turbulent flux at the surface is always upward and the mean turbulent flux at the base of the layer is downward. These assumptions cause  $\wedge \cdot \{(WT)_0\} = (WT)_0$ , so equation (16) becomes

$$(18) \quad (WT)_{-H} = - \wedge \cdot \{ (((1+K) \cdot m \cdot (WSTAR**3)) / (\alpha \cdot g \cdot H)) + K \cdot (WT)_0 - S(F,H) \}$$

The next step is to write every term in equation (18) into a mean plus an anomaly,

$$(19) \quad \overline{(WT)_{-H}} + \underline{(WT)_{-H}}' = - \cdot \{ (((\overline{(1+K)} \cdot \underline{m}) \cdot (WSTAR**3/\overline{H})) / (\alpha \cdot g)) + K \cdot (WT)_0 - S(\overline{F}, \overline{H}) + (((\overline{(1+K)} \cdot \underline{m} \cdot (WSTAR**3/\overline{H}))') / (\alpha \cdot g)) + K \cdot (WT)_0' - S'(\overline{F}, \overline{H}) \}$$

and then substitute into equation (19) for the mean terms in the brackets on the right hand side and subtract  $(WT)_{-H}$  from both sides to get the following form for the anomalous entrainment heat flux.

$$(20) \quad (WT)'_{-H} = - \bigwedge \cdot \{ -(\overline{WT})_{-H} + (((1+K) \cdot m \cdot (WSTAR^{**3}/H)') / (\alpha \cdot g)) + K \cdot (WT)'_0 - S' (F,H) \} - (\overline{WT})_{-H}$$

Expanding the anomaly of a ratio, as in the  $(WSTAR^{**3}/H)'$  term in equation (20), and neglecting the other terms (surface heat flux and solar radiation), equation (20) can be written as

$$(21) \quad (WT)'_{-H} = - \bigwedge \cdot \{ -(\overline{WT})_{-H} + (((1+K) \cdot m \cdot (\overline{WSTAR^{**3}})) / (\alpha \cdot g \cdot \overline{H})) + (((\overline{WSTAR^{**3}})' / (\overline{WSTAR^{**3}})) - (H'/\overline{H})) \} - (\overline{WT})_{-H}$$

The final form necessary for the computer mixing model necessitated one more assumption. The climatological entrainment heat flux at the base of the layer balances much of the surface warming and is of the following form (Wyrтки, 1981),

$$(22) \quad \overline{(\overline{WT})}_{-H} = - .75 \cdot Q_0,$$

where  $Q_0$  is the total downward heat flux at the sea-surface under climatological conditions. This means that  $(\overline{WT})_{-H}$  is generally negative, causing active entrainment and a downward flux of heat at the base of the layer in a long term climatological sense.  $Q_0$  is the net surface heating of the ocean and is obtained from Weare's Atlas (1980). Using a least squares fit on the mean climatological data,  $Q_0$  was found to be 48.14 W/m<sup>2</sup> at the western boundary and 83.00 W/m<sup>2</sup> at the eastern boundary. The computer model required  $Q_0(x)$  for 201 grid points along the equator, and therefore a straight line was fitted between the above two boundary values.

Substituting (22) into (20), gives the final form of the anomalous entrainment heat flux as



$$(23) \quad (WT)'_{-H} = - \bigwedge \cdot \{ .75 \cdot Q0 + (((1+K) \cdot m \cdot \text{ABS}(\bar{U}^{**3})) / (\text{ALPHA} \cdot g \cdot \bar{H})) \cdot (((\text{RHOA} \cdot \text{CD}) / \text{RHOSEA})^{**1.5}) \cdot (((3 \cdot U') / \bar{U}) - (H' / \bar{H})) \} + .75 \cdot Q0$$

RHOA is the air density, RHOSEA is the density of sea water, and CD is the drag coefficient.  $U'$  is the computed anomalous wind, and  $\bar{U}$  is the mean wind as a function of latitude.  $H'$  is the pycnocline anomaly computed by the model and  $\bar{H}$  is the sloping pycnocline previously discussed.

The key terms of equation (23) are  $U'$  and  $H'$ . Isolating the effect of a positive zonal wind anomaly (Fig4.6) superimposed upon a negative mean zonal wind ( $0 < U' < 1$ ), where  $\bar{U} = -5\text{m/sec}$ , it can be seen that the value of  $(U'/\bar{U})$  is less than zero. For  $\bigwedge = 1$  (ie.  $Q0$  dominating all anomalies in the brackets), this produces a positive value of  $(WT)'_{-H}$  and, according to (12), a warming of the sea-surface temperature anomaly. This results because for this particular case (ie.  $U'/\bar{U} < 0$ ) the total wind speed is reduced, which implies weaker mixing than normal. If the sign of  $U'$  and  $\bar{U}$  were the same, then the total wind speed would be larger than normal, there would be greater mixing, and hence cooling of the SST anomaly.

The same investigation can be done for the physical effect of  $H'$ .  $H'$  is computed by the model and can be positive or negative. In the case where  $H'$  is larger than zero, the total pycnocline depth is deeper than the normal  $\bar{H}$ .  $H'/\bar{H}$  is greater than zero, and the overall sign of  $(WT)'_{-H}$  is greater than zero (see equation (23)). The interpretation of this result is that when the pycnocline depth is greater than normal, the normal wind effects cannot reach the base of the layer and cause the normal amount of turbulent mixing of cold water from below. The result is that the layer will be cooled less than normal. In other words, it will warm. If

$H'$  is less than zero, the pycnocline is shallower than normal  $\bar{H}$ . Then the layer will be more effected by the wind than normal, and therefore turbulence will cause more than normal entrainment, and hence the layer will experience anomalous cooling. It is these effects of vertical turbulent mixing which are to be investigated along with zonal advection (equation 12).

### III. RESULTS AND OBSERVATIONS

#### A. EFFECTS OF HORIZONTAL ADVECTION ONLY (CASE ONE)

The control run for this thesis is the horizontal advection case (Rennick, 1985) along with the refinements described in Chapter II. This means that the entrainment mixing term in (12) and the  $We'$  term in (13) were set to zero. The ocean model was integrated for a total of five hundred days, forced by the Blundell and Gill wind patch (5), with the following results.

The pycnocline anomaly will be analyzed first due to its impact on the currents. Figures 4.7-4.11 show a sequence of "snap shots" at fifty day intervals of the current and pycnocline depth anomalies. The length of the arrows denotes the current speed in meters per second. Contour intervals and length scales are defined for each panel. The solid contours imply a positive pycnocline anomaly and therefore a deeper pycnocline than normal. The dashed contours are negative pycnocline anomalies which indicate a shallower layer than normal. Figure 4.7 shows an classical example of a propagating Kelvin wave in that the maximum zonal current and maximum pycnocline anomaly locations coincide. Away from the equator, the flow is parallel to the isobars and is in geostrophic balance with the north/south pressure gradient. The movement of the pycnocline anomaly contours to the east is very rapid and corresponds very well with the propagation speed of the wind patch (approximately .32m/sec).

Figure (4.8) shows the Kelvin wave spreading north and south along the eastern boundary. At this point, a reflection back towards the west is evident. This continues to

intensify in Figure (4.9). The surface layer in the western ocean is continuing to shallow, and at day three hundred (Figure 4.9) the shallowing has reached as far east as  $130^{\circ}$  west longitude.

Figure (4.10) shows the formation of an easterly jet along the equator. The hint of a Rossby wave to the north and south of the jet can be intimated. Since the Rossby wave moves so much more slowly than the Kelvin wave, more time is required to infer its actual motion. By day four hundred the formation of anticyclones (highs) to the north and south of the jet can be seen along with an intensification of the easterly jet caused by the Rossby waves.

The Rossby wave motion becomes more obvious in Figure 4.11. The westward movement of the anticyclones corresponds well with the Rossby wave speed. At day four hundred fifty (upper panel) the first indications that the pycnocline is shallowing at the eastern boundary become evident. This is due to the easterly jet and the cessation of the anomalous winds (see Figure 4.6). In order to better see the full structure of the Rossby waves, the model boundaries need to be more than  $15^{\circ}$  of latitude from the equator. The upper boundaries are causing interference, but a maximum in the anticyclones to the west in both panels still allows development of the Rossby wave. The Rossby wave causes the easterly jet, the shallowing of the pycnocline, and the cooling of the sea surface from the east (see Figures 4.15-4.16).

Figures 4.12-4.16 are the results for SST anomaly. A sequence of figures at fifty day intervals for the five hundred days is presented. Solid contours indicate positive SST anomalies and dashed contours negative SST anomalies. Contour intervals are specified above each panel and are in units of degrees centigrade.



Figure 4.12 demonstrates that the SST anomaly also propagates at the same speed as a Kelvin wave ( 2-3 m/sec.). By day one hundred, almost the entire basin along the equator has experienced some warming due to the anomalous advection of warm water from the west by the anomalous zonal currents of the Kelvin wave. An approximation in the Pacific is that a Kelvin wave will cross the basin in approximately one hundred days. This is supported by the lower panel in Figure 4.7, where it can be seen that the deepening of the pycnocline is already beginning at one hundred days. The values of the SST anomaly are very small and would be an observationalist's nightmare, but they are not random.

Interaction with the eastern boundary is evident in Figure 4.13 (lower panel). The flattening of the contours at day two hundred implies that the Kelvin wave is reflecting from the boundary. In Figure 4.14 (lower panel) the Kelvin wave is moving north and south along the boundary. It should also be noted that temperatures peak near day two hundred fifty, and then they begin to decrease.

The cooling from the eastern boundary continues in Figure 4.15, and at day four hundred the effect of the westerly jet caused by the Rossby waves is clearly evident. Figure 4.16 continues to show the effect of the easterly jet as cooling extends to  $145^{\circ}$  west longitude on day four hundred fifty. At this time the easterly wind patch ceases (see Figure 4.6), and cooling extends to  $150^{\circ}$  east longitude by day five hundred (lower panel).

The zonal movement along the equator can better be seen using a time-longitude plot; therefore, Figures 4.17 and 4.18 have been included. Solid contours are positive anomalies, and dashed contours are negative anomalies.

The Kelvin wave front is well demonstrated in the pycnocline depth anomaly at the eastern boundary by the rapid

increase followed by a rapid decrease (Figure 4.17). The decrease ( $dH'/dt < 0$ ) after day three hundred is caused by the north/south propagation of the Kelvin wave after it has reached the boundary. The zonal speed of the disturbance may be inferred from the slope of the  $H' = 0$  line and is approximately .32 m/sec, which is equivalent to the speed of the wind patch.

Basin wide warming is the trend shown in Figure 4.18. After day four hundred negative anomalies occur due to the easterly jet previously discussed. The cutoff of the winds at four hundred fifty days is also a factor.

## B. EFFECTS OF MIXING ONLY (CASE TWO)

For case two, the zonal advection term in the SST anomaly equation (12) was excluded, and the entrainment mixing term was included. Also, the  $We'$  term was added to equation (13). Similar runs were made as in case one, but only differences in results will be discussed here.

The SST anomaly patterns in case two were very different from those in case one. The amplitude of the anomaly is very small but well organized. Figures 4.19-4.23 display the same time "snap shots" as those done in case one Figures 4.12-4.16, in the results.

The SST anomaly does not propagate eastward with the Kelvin wave speed of 2-3 m/sec as in case one. Instead the progression of the SST anomaly maximum is a wind-forced response with a speed of approximately .32 m/sec. The meridional extent of the SST anomaly field is also much larger than that of case one, even though its magnitude is an order or two smaller. The peak SST anomaly is attained at day three hundred (Figure 4.21). The wind patch and its associated SST anomaly field continues to move eastward (Figures 4.22-4.23) until day four hundred fifty, when the wind patch

ceases and cooling commences at the eastern boundary. No negative SST anomalies ever develop in this case. The difference between case one (Figure 4.16) and case two (figure 4.23) is striking.

The major feature in the SST anomaly field is the phase difference it has with the height field. The height field is traveling at the same speed as the SST anomaly field. The speed of the SST anomaly was computed by measuring the slope of a line through the maximums of the SST anomaly field in Figure 4.24.

Rennick and Haney (1985) computed that the phase difference should be  $90^\circ$  for a free wave, but in the forced case it is less than that. Comparing the location of the height field maximum (Figure 4.7, lower panel) with that of the SST anomaly maximum (Figure 4.12, lower panel), a phase difference of approximately  $50^\circ$  was obtained.

Although the SST anomalies in case one and two are very different, the pycnocline depth anomaly in the two cases are virtually identical. This is clearly seen in comparing Figure 4.17 with Figure 4.25. An important conclusion concerning the height field can be made from this result because the only difference between case one and two was due to the entrainment mixing parameter  $We'$ . Since no significant difference was evident in the two pycnocline anomaly fields it can be concluded that  $We'$  is negligible. Thus, the evolution of the pycnocline depth anomaly field is controlled by the dynamics of a non-entraining layer. Since the SST anomaly produced by anomalous entrainment mixing is an order or two of magnitude smaller than the advectively produced SST anomalies, the total SST anomaly from equation (12) will be almost identical to that determined by advection alone. This conclusion would be final, if not for the different SST anomaly patterns produced by the two processes.

### C. HORIZONTAL ADVECTION PLUS MIXING (CASE THREE)

From the two previous cases it would be expected that for the linear model being used, a summation of the two fields will not differ much from case one. The final question then to ask is, "could the phase difference in case two have significant effect in a coupled air ocean model?". Even though the SST anomaly in case two is much smaller, a coupled atmosphere-ocean version could experience a factor of one hundred in the growth rate. Therefore, a one percent effect as seen in the uncoupled version could be magnified in a couple system and have an effect. This will be examined in the following cases.

### D. COUPLED MODE WITH HORIZONTAL ADVECTION OF SST (CASE FOUR)

In case four an examination of horizontal advection in a coupled model is made. The question concerns whether growth will occur. The initial conditions for this case are defined by the first one hundred days of case one (Figures 4.7 and 4.12). Thus, the model is first run in a prescribed atmosphere mode for one hundred days, and the ocean is allowed to respond to the atmospheric forcing (Figures 4.1-4.6). At day one hundred the atmosphere is released and allowed to respond to feedback provided by the ocean. The feedback of atmospheric heating is parameterized solely in terms of the SST anomaly predicted by the ocean model.

Figure 4.26 demonstrates that the anomaly initially propagates with the wind patch, but that after day one hundred it rapidly increases in speed. The rapid increase is due to the Kelvin wave which is produced by the initial cut-off of the atmosphere forcing. The layer depth increases until approximately one hundred and fifty days when the Kelvin wave reaches the boundary. At this point in



time the entire basin begins to relax. The lack of growth is caused by the lack of a positive feedback. The SST anomaly which produces the convective heating in the atmosphere simply does not develop a phase relation with the wind which is needed to produce a positive feedback. This result is consistent with the analytic findings in Rennick and Haney (1985) and the numerical study of Rennick (1985). Therefore, the conclusion can only be that horizontal advection of SST with dynamic forcing in itself cannot cause the growth exhibited in ENSO.

Figure 4.27 shows the same initial growth of SST anomaly as in 4.18 of case one for one hundred days. Supporting the findings in Figure 4.26 there is eastward propagation of the SST anomaly followed by relaxation of the entire basin. As previously stated, no positive feedback develops, and therefore there is no growth.

#### E. COUPLED MODE WITH TURBULENT MIXING ONLY (CASE FIVE)

The previous case supports the hypothesis that no growth will occur when SST is governed by horizontal advection alone. Here an investigation is made concerning whether the different phase of the SST anomaly produced by anomalous mixing can tip the balance and cause growth. The model is initialized by repeating the first one hundred days of Case Three. After one hundred days the atmosphere is allowed to interact with the ocean, and the results are displayed in Figures 4.28-4.29.

Comparing Figure 4.28 with 4.17, a large difference in propagation of the pycnocline anomaly is seen. Figure 4.17 is the same for Cases One and Two and showed that the propagation speed is equal to that of the wind patch speed. This can be seen for the first one hundred days in Figure 4.28, but after one hundred days a rapid change in phase speed

occurs and is equivalent to the Kelvin wave speed. Thus, at day one hundred, a pulse is generated by the cut-off of the prescribed winds and it traverses the basin at the Kelvin wave speed (2-3m/sec). At the eastern boundary, the depth increases until the Kelvin wave reaches the boundary, and then the anomaly begins to decay. There appears to be no feedback or growth of any kind after one hundred and sixty days. The coupled system simply spins-down.

Figure 4.29 is the SST anomaly at the equator for five hundred days. The difference of a factor of five in contour intervals also supports the results shown in Figure 4.28. There is no feedback or growth after one hundred days. The major result is that the phase difference of the mixing case does not cause any growth by itself, and if added to the horizontal advection case, still no growth would be experienced.

#### IV. CONCLUSIONS

The analysis of the anomalous entrainment mixing shows that in a linear ocean model and in a coupled ocean-atmosphere model, entrainment can be ignored as a growth mechanism for ENSO. The phase difference in the SST anomalies produced was not able to overcome the large difference between the horizontal advection case and the mixing case.

The investigation of other terms in equation (11) must be investigated in order to understand fully the SST response to forcing from the atmosphere in equatorial regions. In this analysis all that was considered was the anomalous entrainment mixing at the base of the layer  $((WT)'_0 / \bar{H})$  and the effects of the wind on this mixing process.

Solar radiation fluctuations have a direct effect on the SST anomaly as well as an effect on the turbulent mixing  $(S'(F,H))$  in equation 20) which has been ignored in this study. These effects could in turn cause anomalous heating or cooling of the atmosphere and have a different phase which may cause the growth associated with the El Nino event.

The anomalous surface heat flux  $((WT)'_0 / \bar{H})$  would logically be the next term to be investigated. This term is difficult to model because it is affected by cloud cover and changes in humidity which are difficult to parameterize, especially in a coupled model. Therefore, a number of ocean-only case studies should be made, using statistical data from the Weare and Strub (1980) Atlas for averaged anomalous heat flux fields.

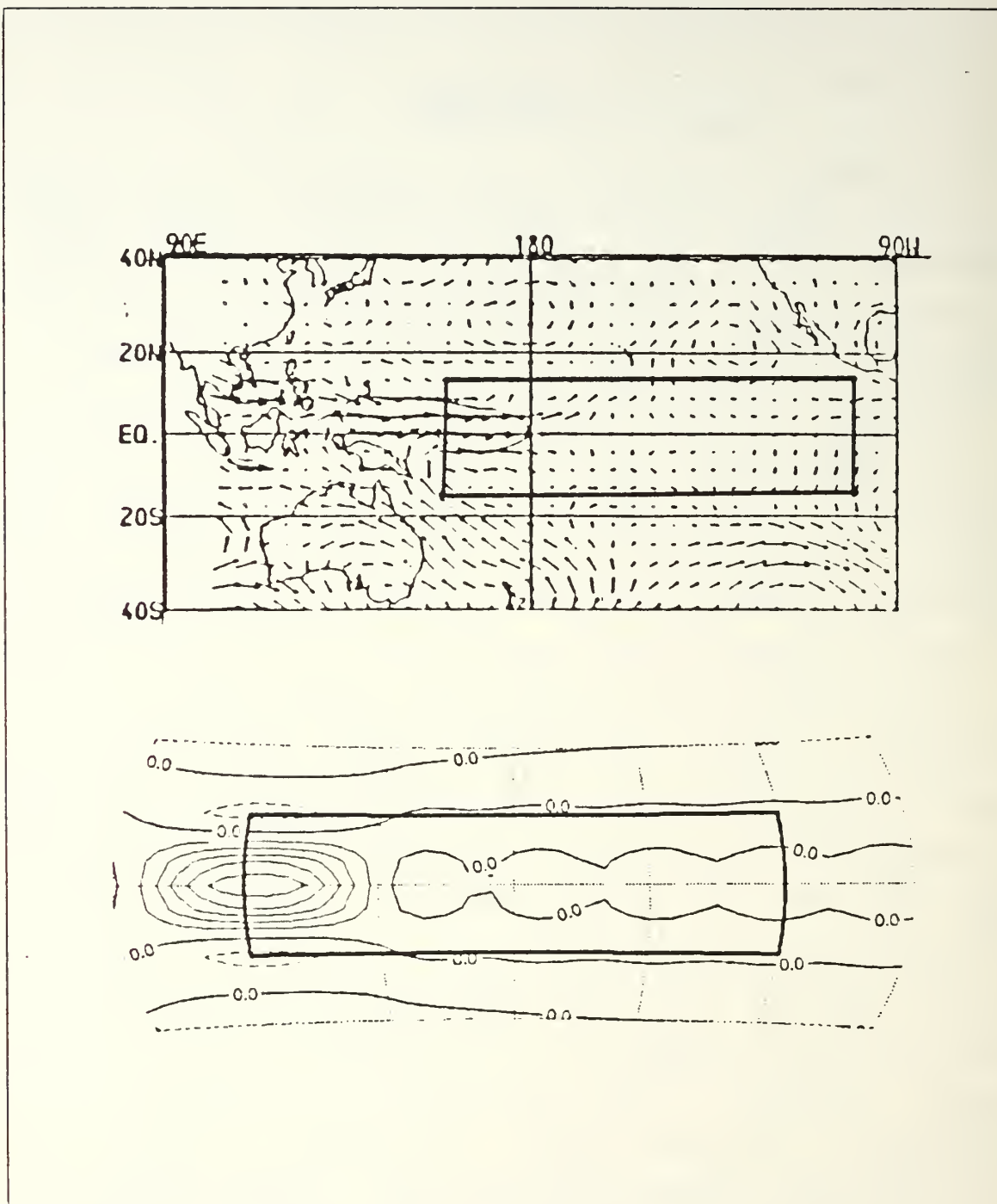


Figure 4.1 Anomalous winds for June, July, August 1982  
 Observed (upper) and computer generated (lower) Q  
 contours 5m/sec (upper) and .2m/sec (lower).

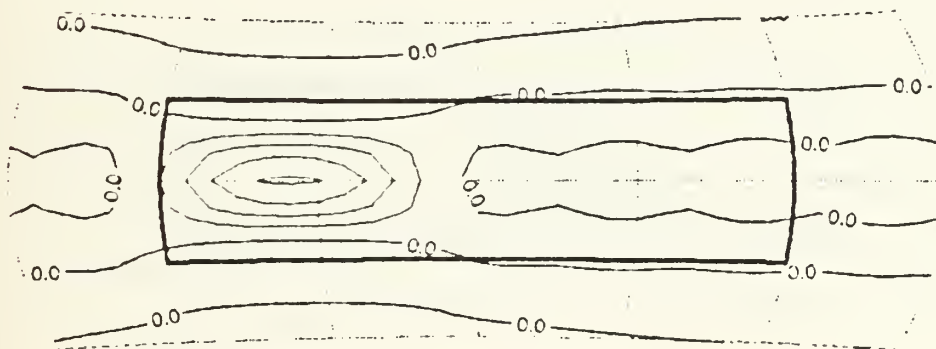
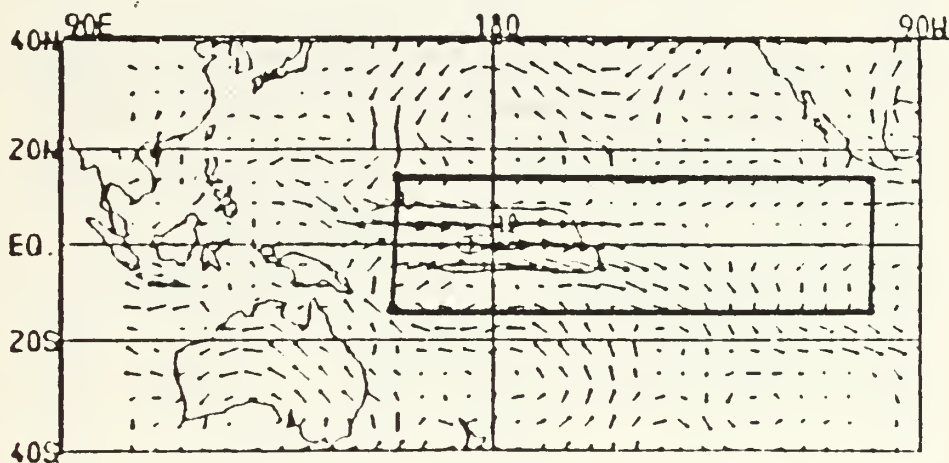


Figure 4.2 Anamolous winds for September, October, November 1982, observed(upper) and computer generated (lower); contours 5m/sec( upper) and .2m/sec(lower).



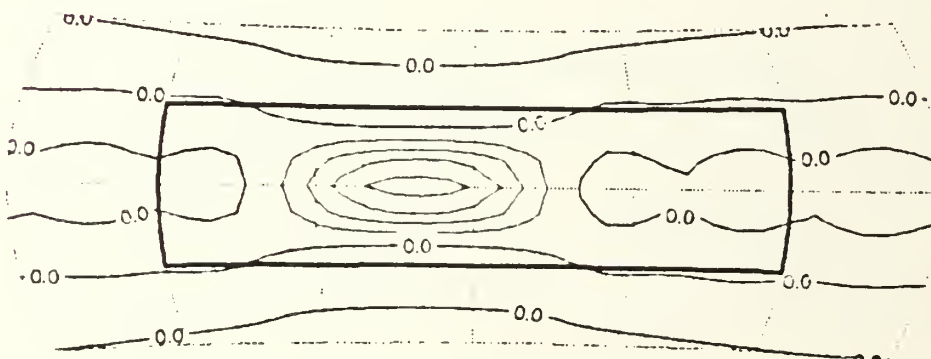
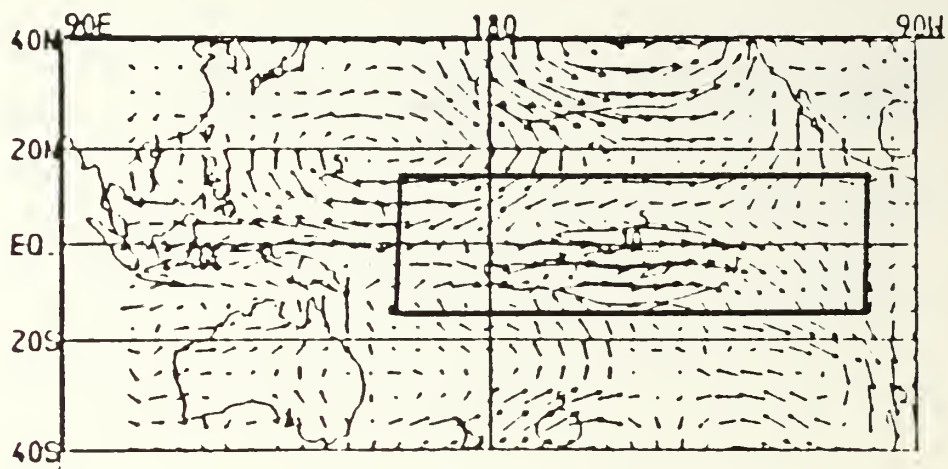


Figure 4.3 Anomalous winds for December, January, February 1982-1983, observed(upper) and computer generated (lower); contours 5m/sec(upper) and .2m/sec(lower).

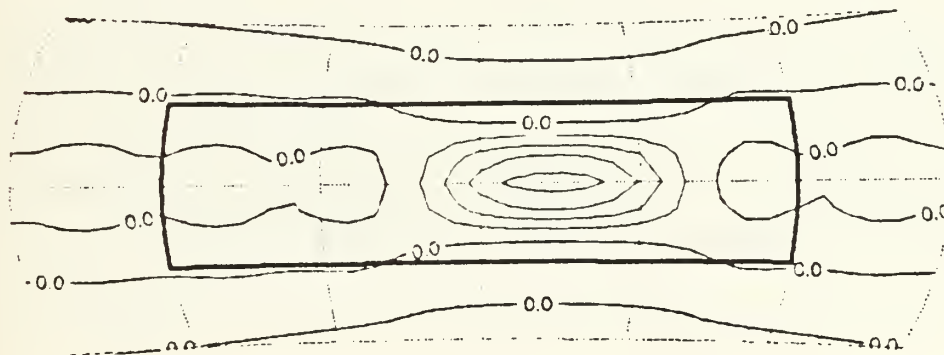
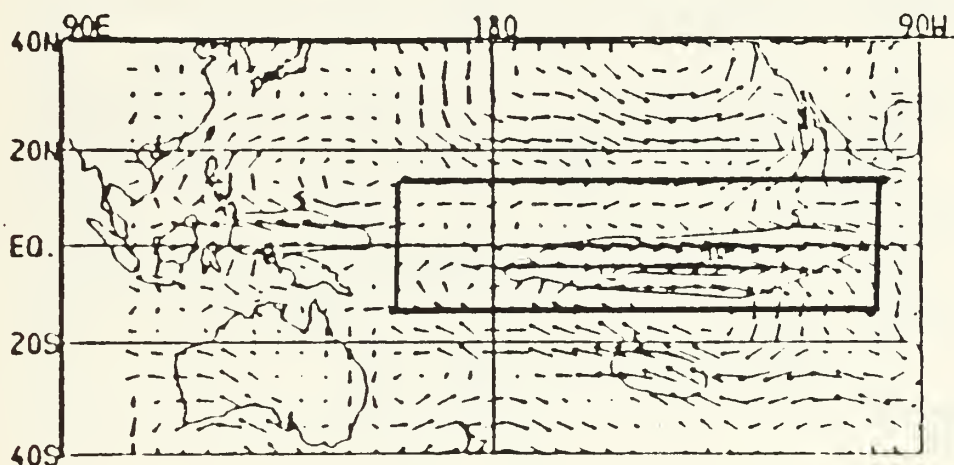


Figure 4.4 Anomalous winds for March, April, May 1983, observed(upper) and computer generated (lower); contours 5m/sec(upper) and .2m/sec(lower).

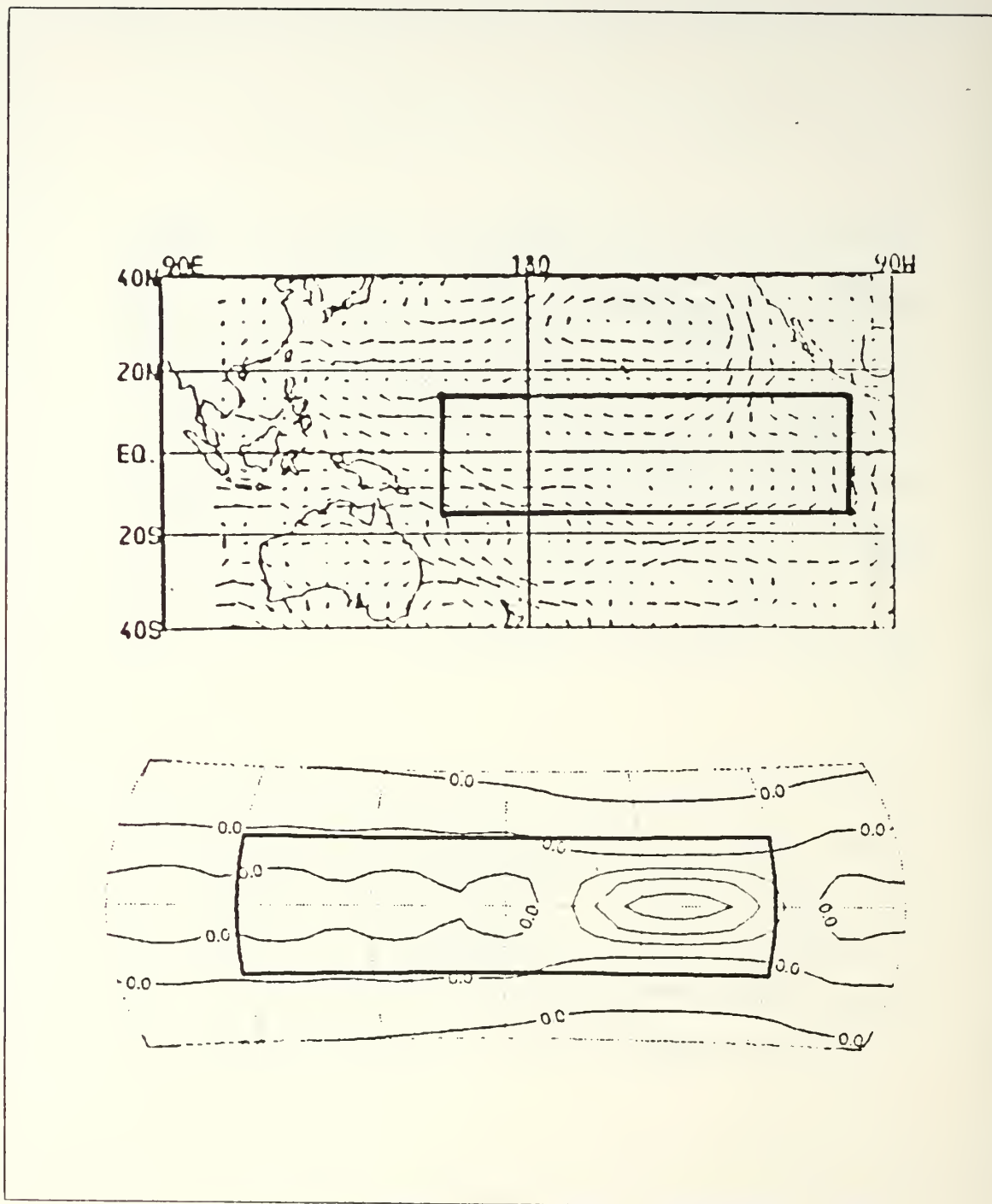


Figure 4.5 Anomalous winds for June, July, August 1983,  
observed(upper) and computer generated(lower);  
contours 5m/sec(upper) and .2m/sec(lower).

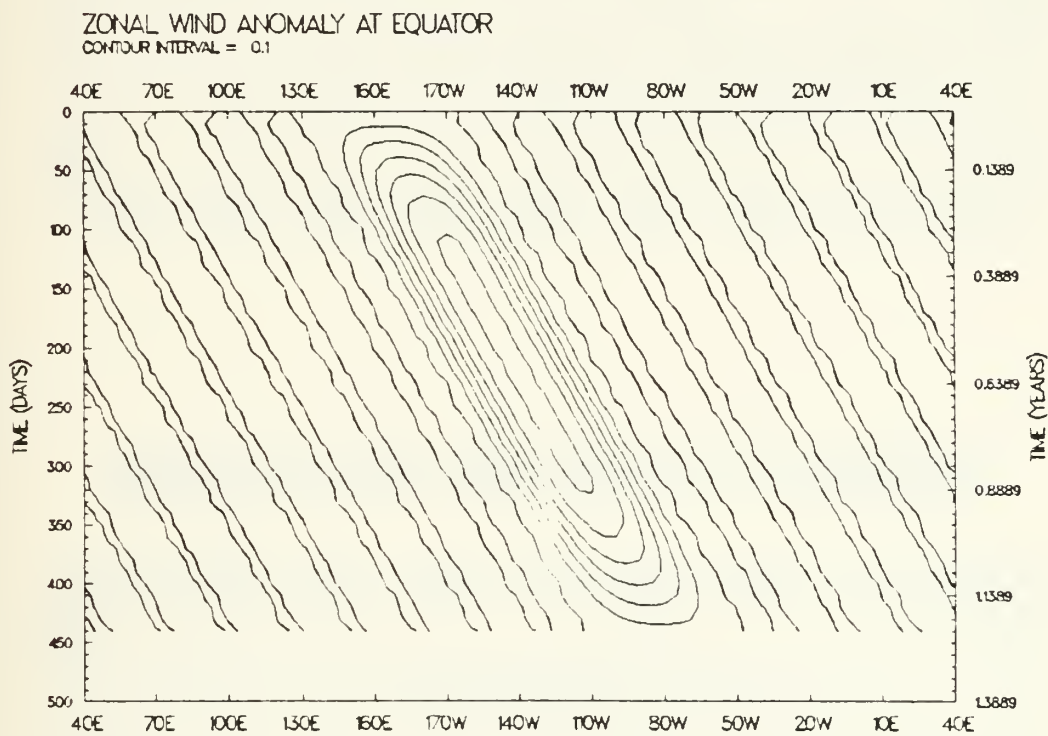
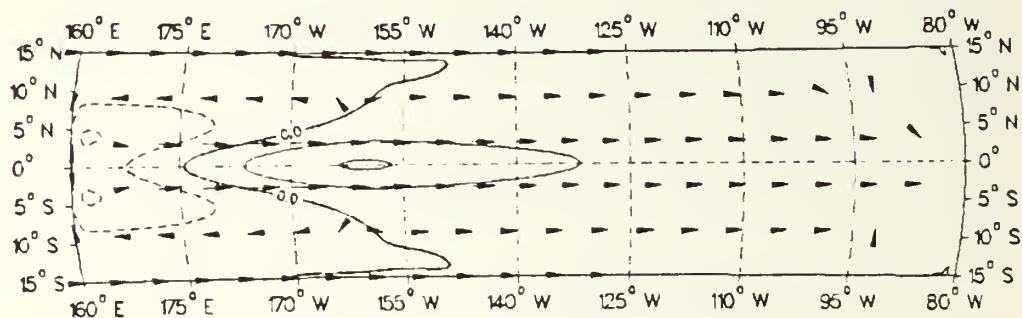


Figure 4.6 Case one, zonal wind anomaly (m/sec)  
time-longitude plot.

# CURRENT AND PYCNOCLINE ANOMALIES AT DAY 50

CONTOUR INTERVAL = 0.5

→ 0.010



# CURRENT AND PYCNOCLINE ANOMALIES AT DAY 100

CONTOUR INTERVAL = 1

→ 0.02

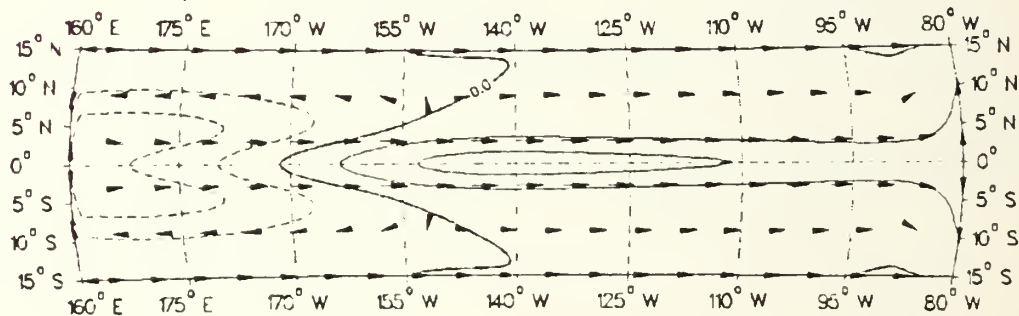


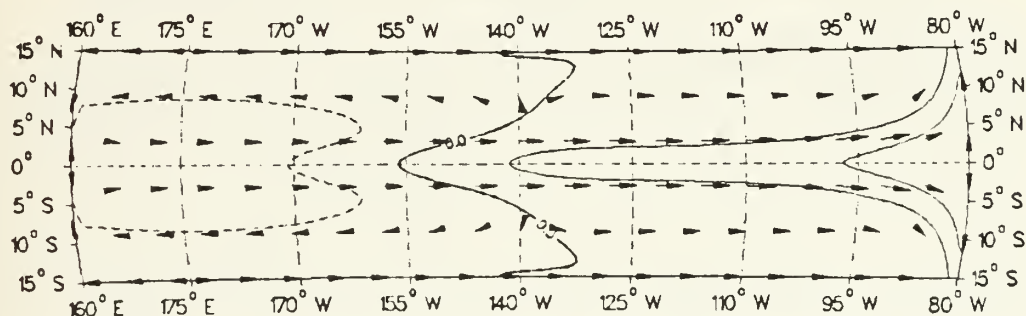
Figure 4.7 Case one, depth (m) and current anomalies (m/sec) for entire basin (day 50 and 100).



# CURRENT AND PYCNOCLINE ANOMALIES AT DAY 150

CONTOUR INTERVAL = 2

→ 0.02



# CURRENT AND PYCNOCLINE ANOMALIES AT DAY 200

CONTOUR INTERVAL = 2

→ 0.02

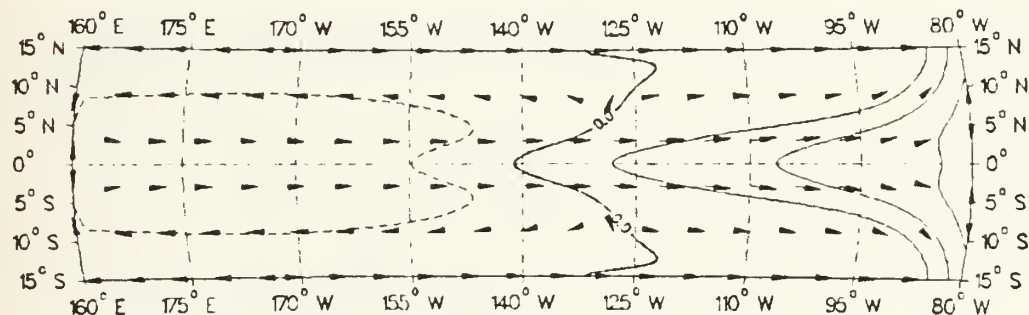
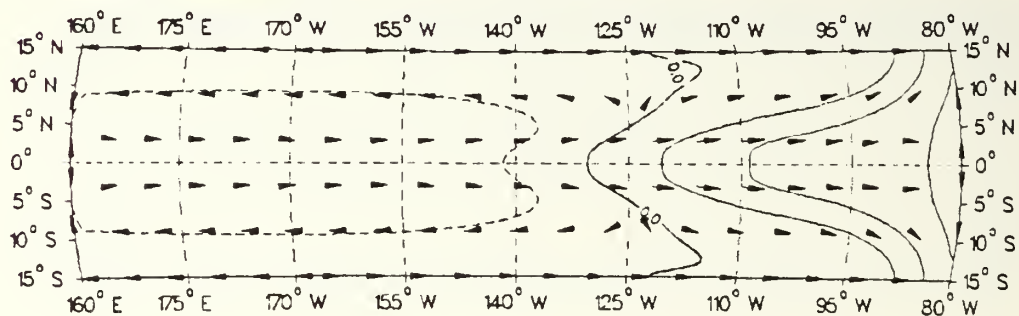


Figure 4.8 Case one, depth (m) and current anomalies (m/sec) for entire basin (day 150 and 200).

# CURRENT AND PYCNOCLINE ANOMALIES AT DAY 250

CONTOUR INTERVAL = 2

→ 0.02



# CURRENT AND PYCNOCLINE ANOMALIES AT DAY 300

CONTOUR INTERVAL = 2

→ 0.02

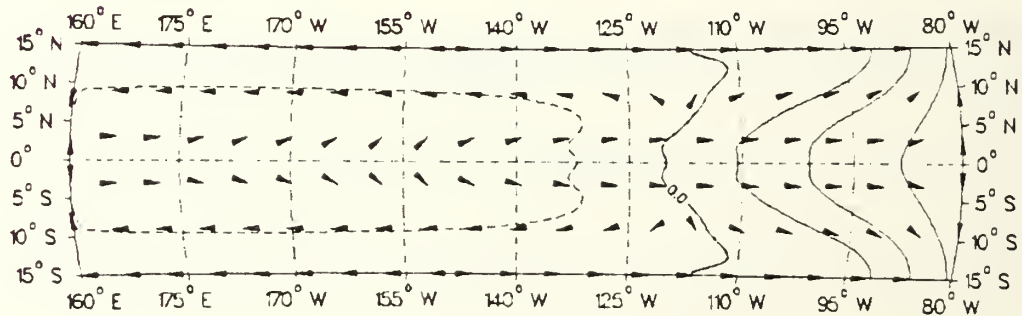
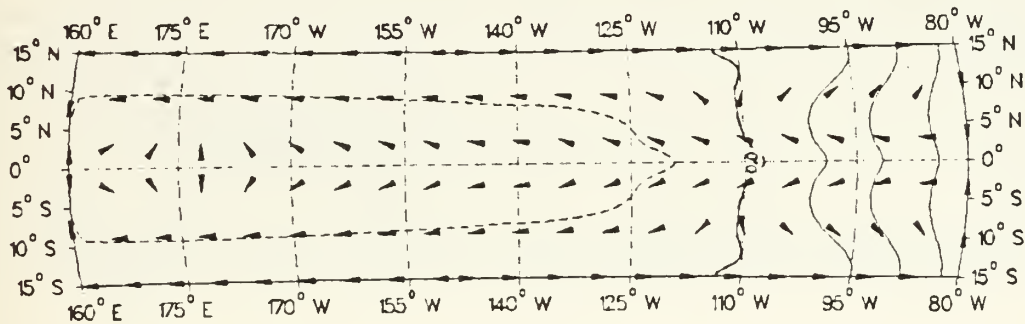


Figure 4.9 Case one, depth (m) and current anomalies (m/sec) for entire basin (day 250 and 300).

# CURRENT AND PYCNOCLINE ANOMALIES AT DAY 350

CONTOUR INTERVAL = 2

→ 0.01



# CURRENT AND PYCNOCLINE ANOMALIES AT DAY 400

CONTOUR INTERVAL = 1

→ 0.02

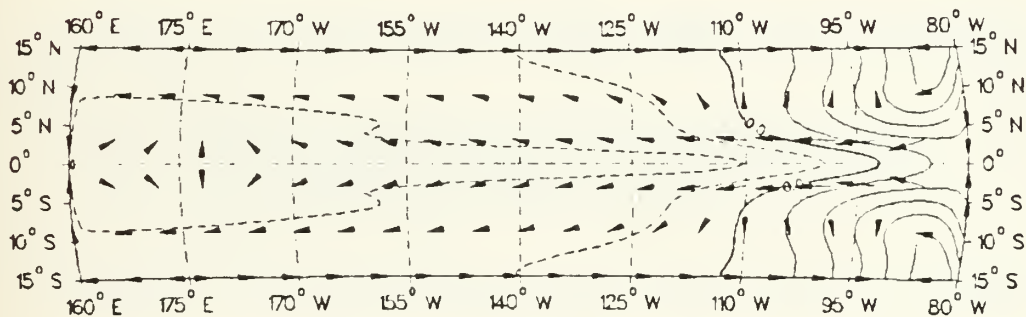
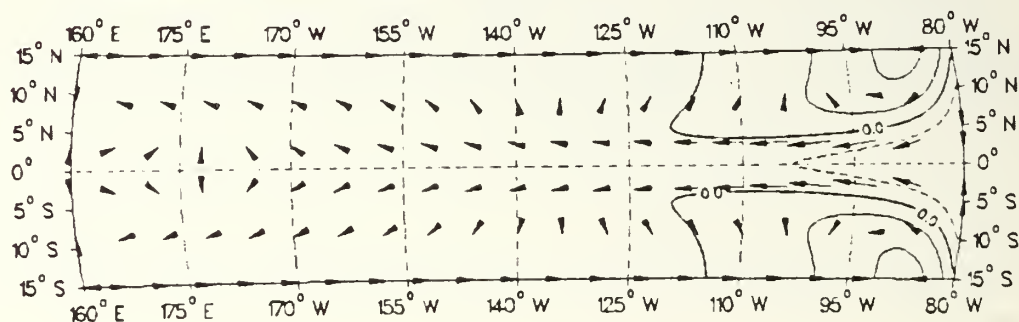


Figure 4.10 Case one, depth (m) and current anomalies (m/sec) for entire basin (day 350 and 400).

CURRENT AND PYCNOCLINE ANOMALIES AT DAY 450  
 CONTOUR INTERVAL = 2      → 0.02



CURRENT AND PYCNOCLINE ANOMALIES AT DAY 500  
 CONTOUR INTERVAL = 1      → 0.02

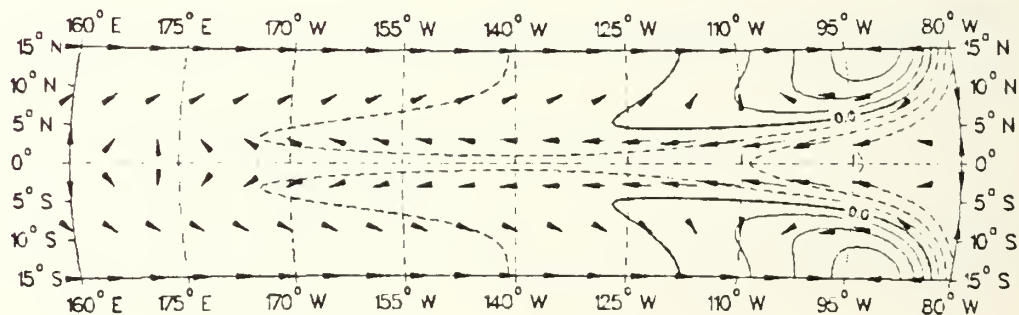
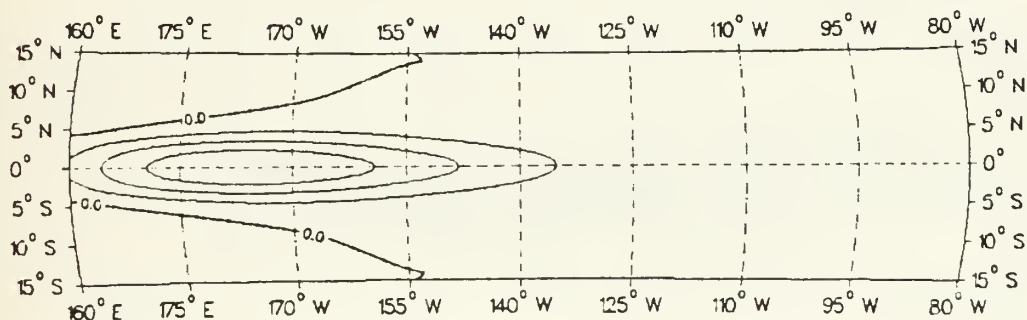


Figure 4.11 Case one, depth (m) and current anomalies (m/sec) for entire basin (day 450 and 500).

# SST ANOMALY AT DAY 50 CONTOUR INTERVAL = 0.002



# SST ANOMALY AT DAY 100 CONTOUR INTERVAL = 0.005

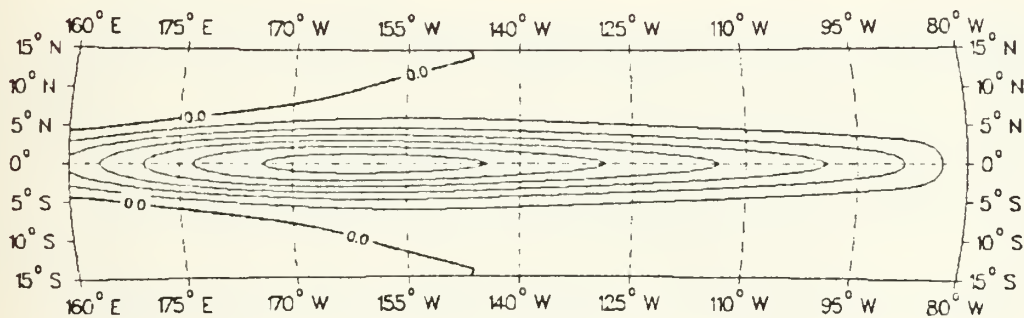
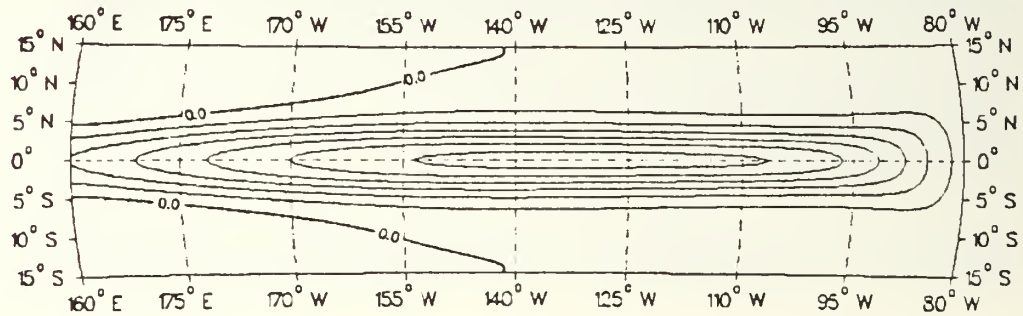


Figure 4.12 Case one, SST anomalies (deg C) for entire basin (day 50 and 100).



SST ANOMALY AT DAY 150  
CONTOUR INTERVAL = 0.010



SST ANOMALY AT DAY 200  
CONTOUR INTERVAL = 0.02

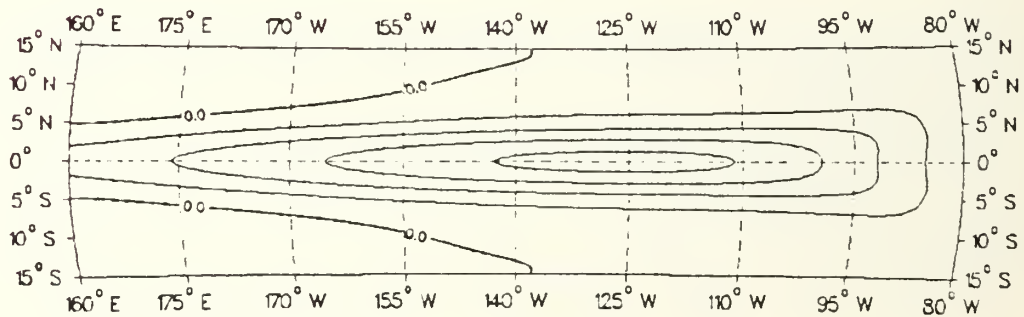
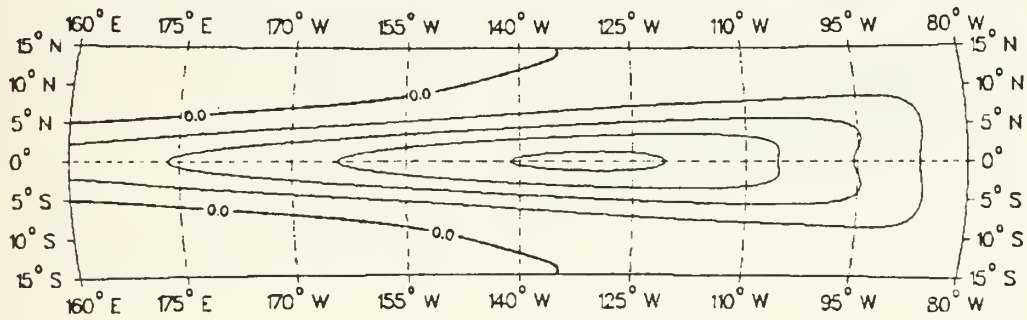


Figure 4.13 Case one, SST anomalies (deg C) for entire basin (day 150 and 200).

SST ANOMALY AT DAY 250  
CONTOUR INTERVAL = 0.02



SST ANOMALY AT DAY 300  
CONTOUR INTERVAL = 0.010

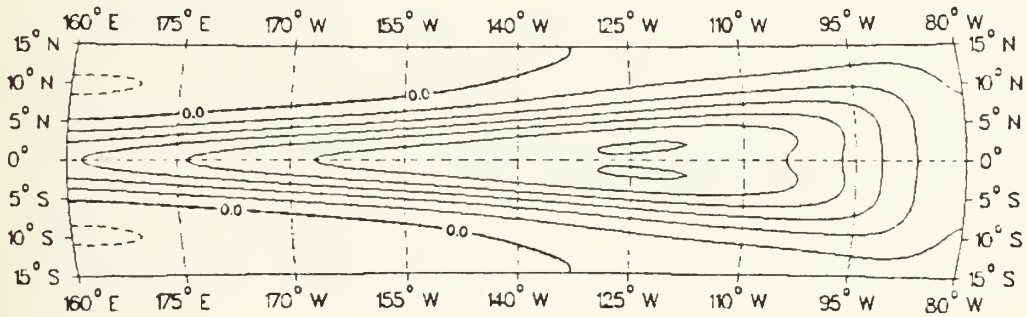
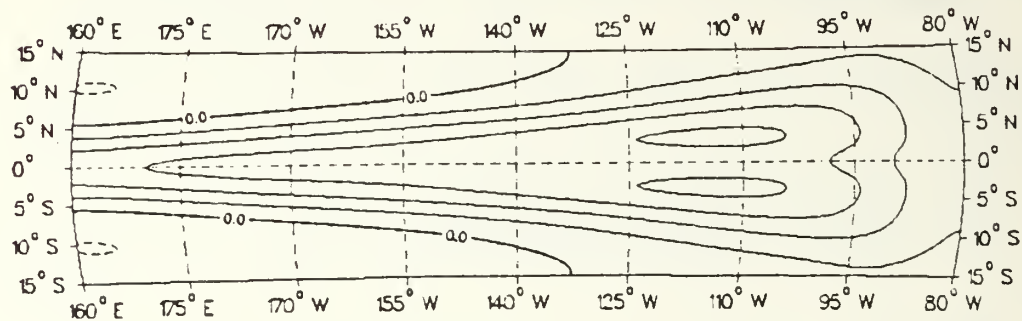


Figure 4.14 Case one, SST anomalies (deg C) for entire basin (day 250 and 300).

SST ANOMALY AT DAY 350  
CONTOUR INTERVAL = 0.010



SST ANOMALY AT DAY 400  
CONTOUR INTERVAL = 0.005

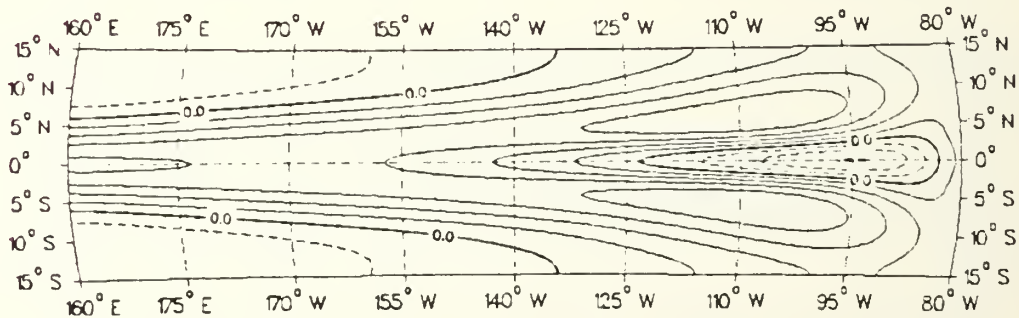
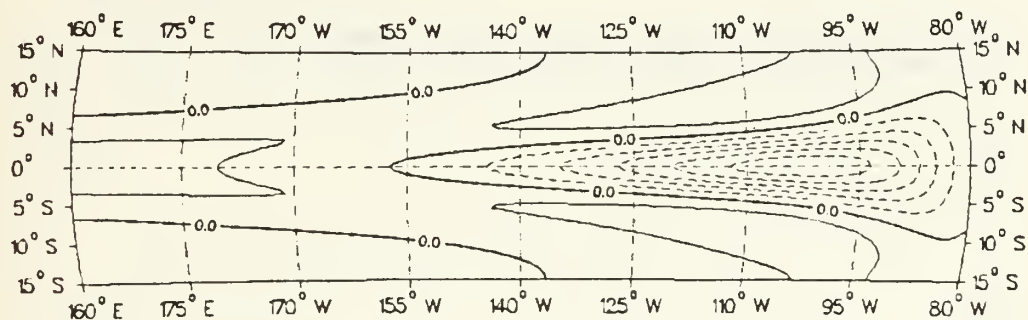


Figure 4.15 Case one, SST anomalies (deg C) for entire basin (day 350 and 400).

SST ANOMALY AT DAY 450  
CONTOUR INTERVAL = 0.010



SST ANOMALY AT DAY 500  
CONTOUR INTERVAL = 0.010

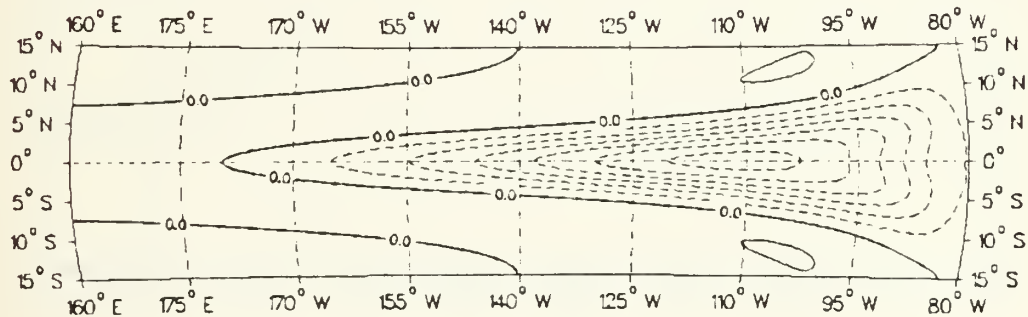


Figure 4.16 Case one, SST anomalies (deg C) for entire basin (day 450 and 500).



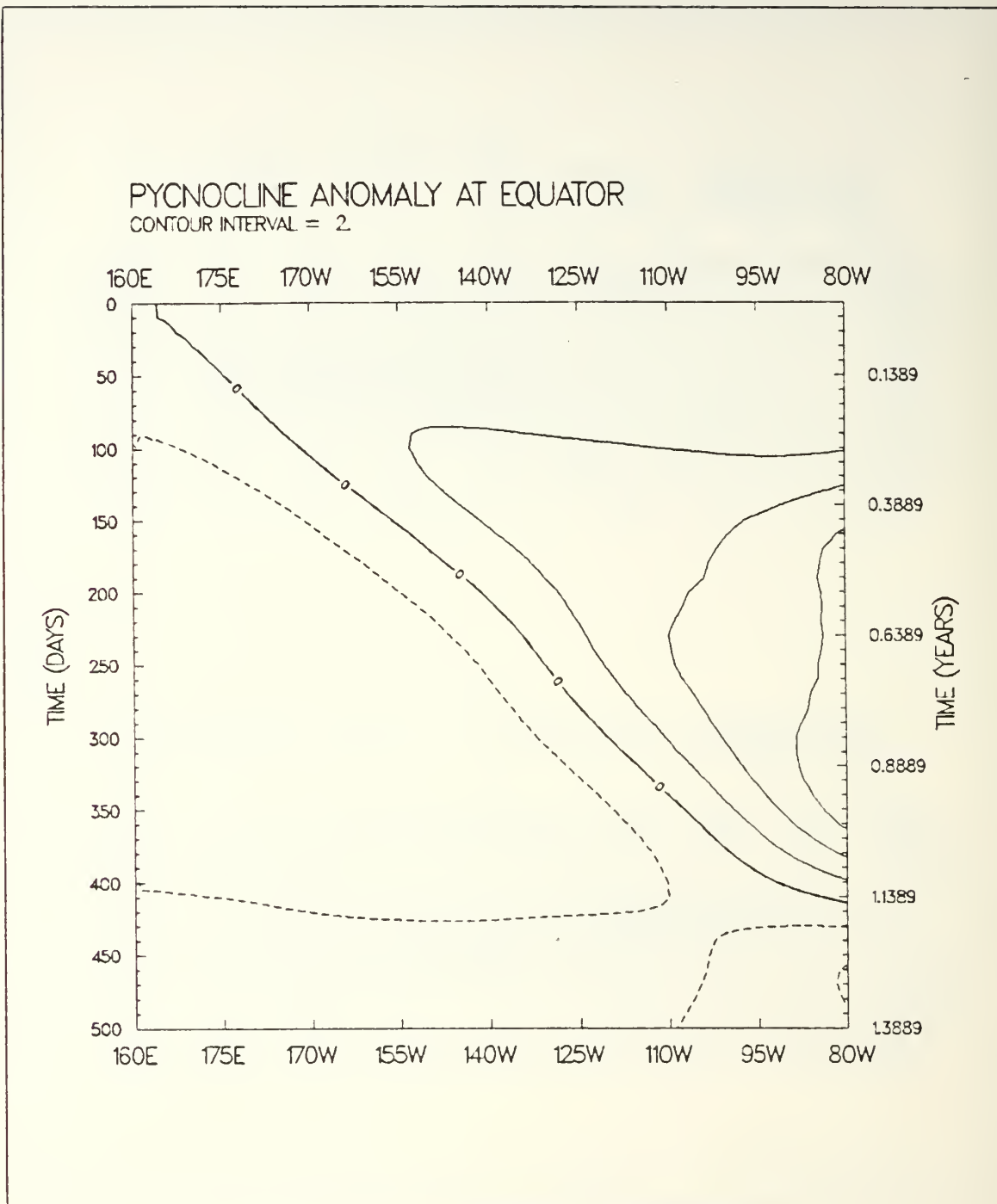


Figure 4.17 Case one, pycnocline depth anomaly (m)  
time- longitude plot.

# SST ANOMALY AT EQUATOR

CONTOUR INTERVAL = 0.02

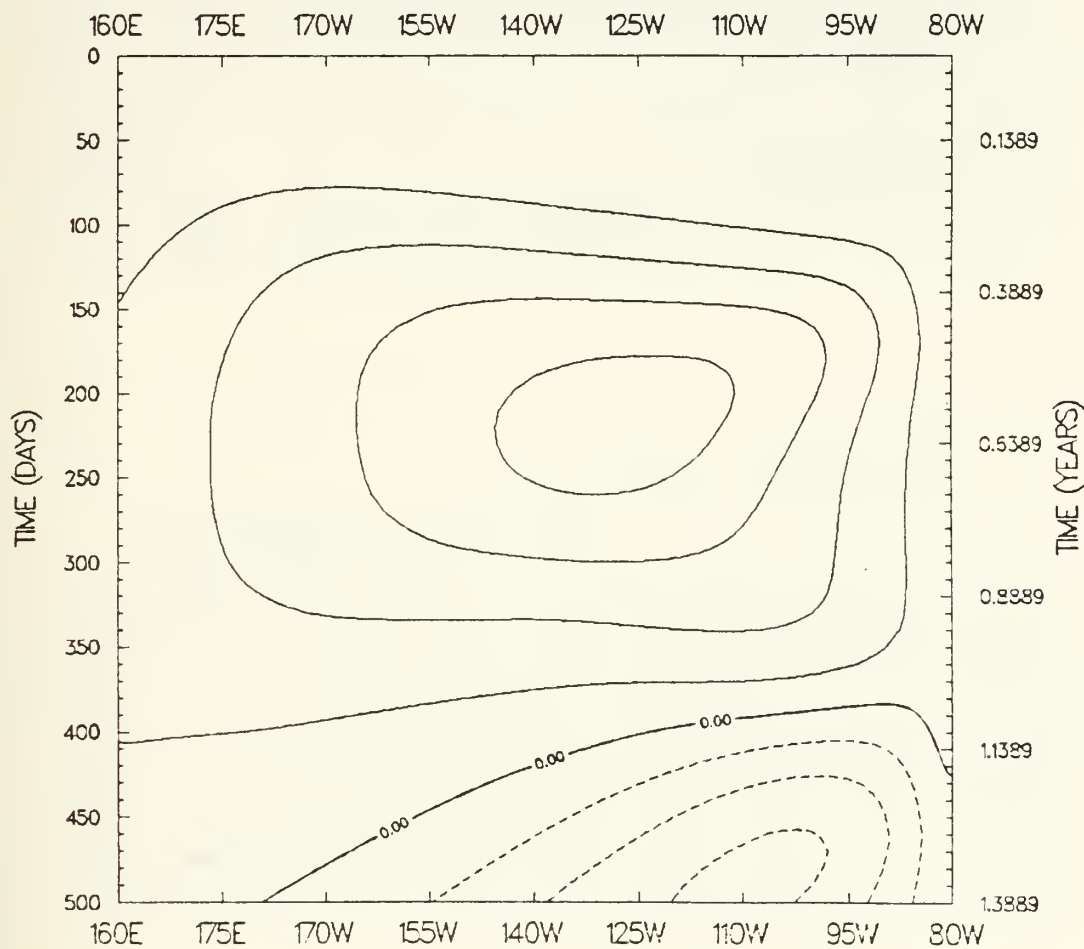
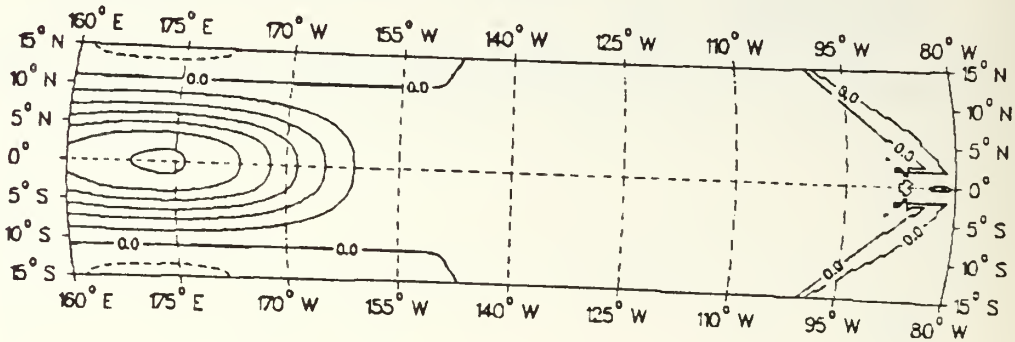


Figure 4.18 Case one, SST anomaly (deg C)  
time-longitude plot.

# SST ANOMALY AT DAY 50 CONTOUR INTERVAL = 0.00005



# SST ANOMALY AT DAY 100 CONTOUR INTERVAL = 0.0002

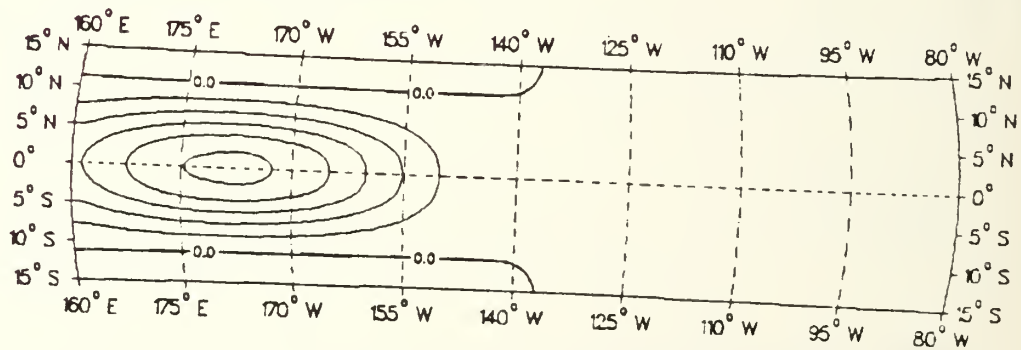
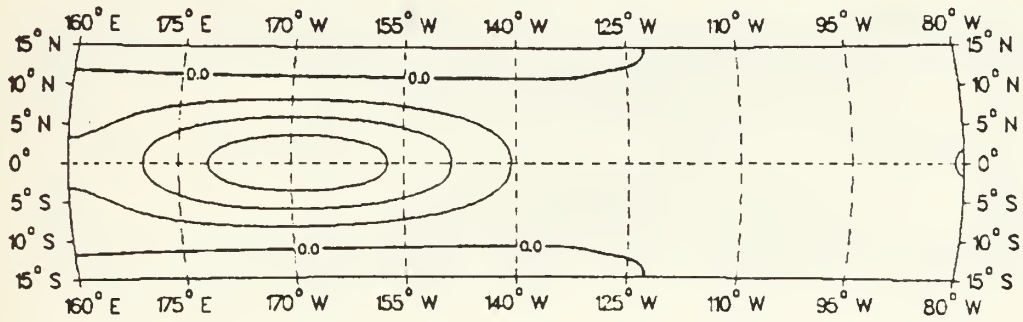


Figure 4.19 Case two, SST anomalies (deg C) for entire basin (day 50 and 100).

SST ANOMALY AT DAY 150  
CONTOUR INTERVAL = 0.0005



SST ANOMALY AT DAY 200  
CONTOUR INTERVAL = 0.0005

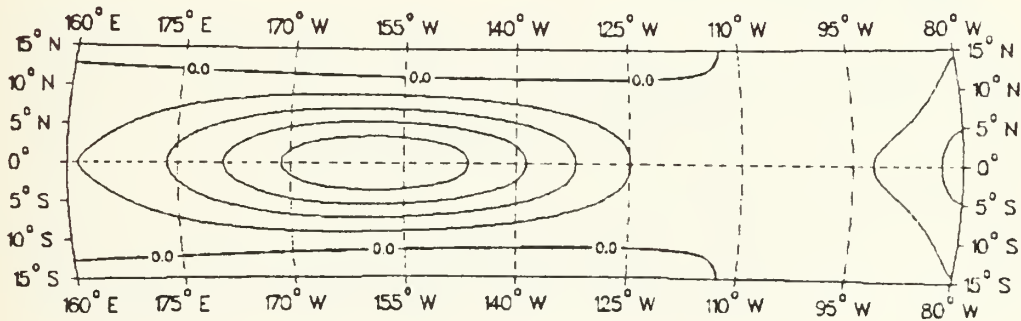
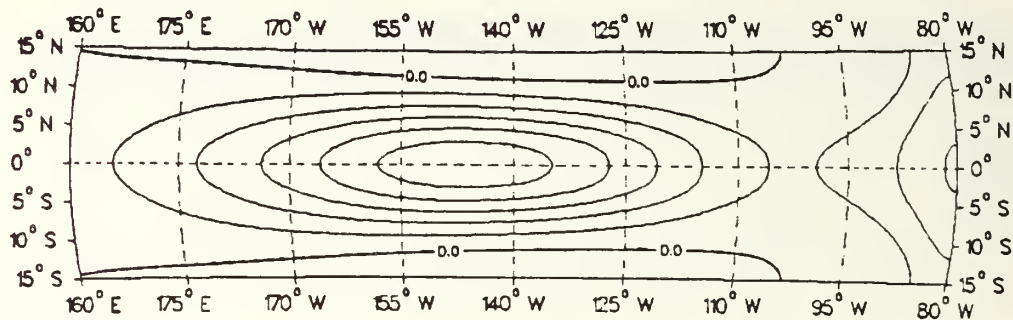


Figure 4.20 Case two, SST anomalies (deg C) for entire basin (day 150 and 200).

SST ANOMALY AT DAY 250  
CONTOUR INTERVAL = 0.0005



SST ANOMALY AT DAY 300  
CONTOUR INTERVAL = 0.0005

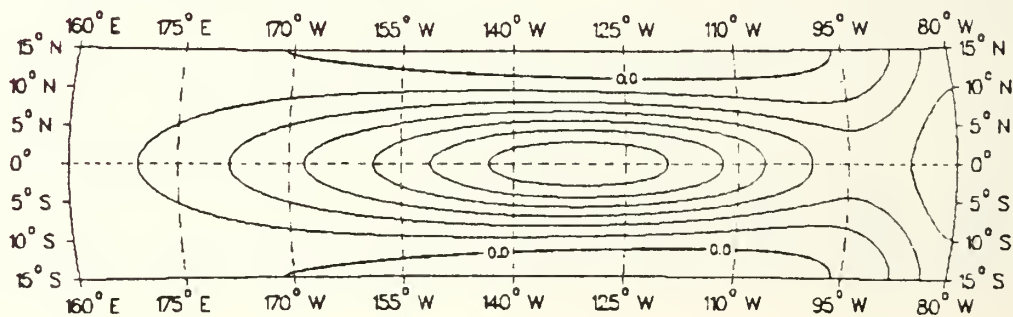
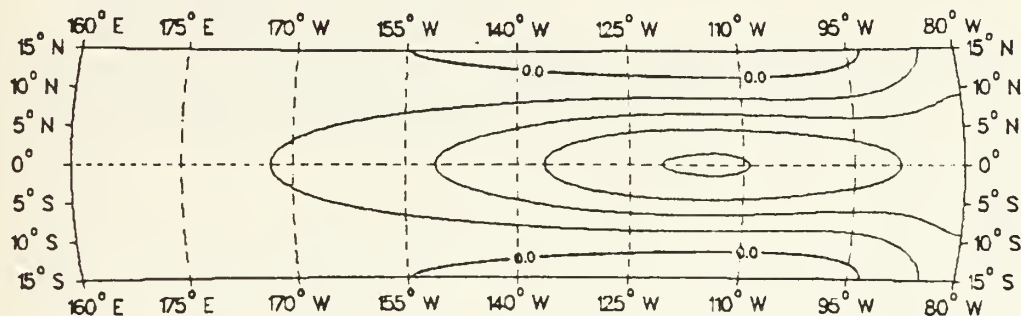


Figure 4.21 Case two, SST anomalies (deg C) for entire basin (day 250 and 300).



# SST ANOMALY AT DAY 350

CONTOUR INTERVAL = 0.0010



# SST ANOMALY AT DAY 400

CONTOUR INTERVAL = 0.0010

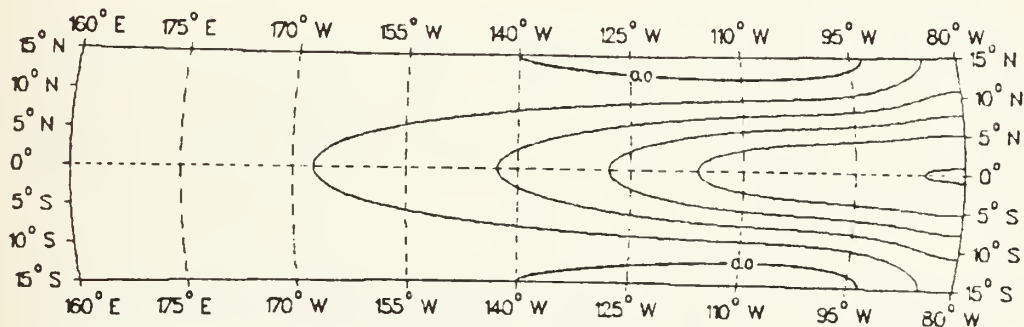
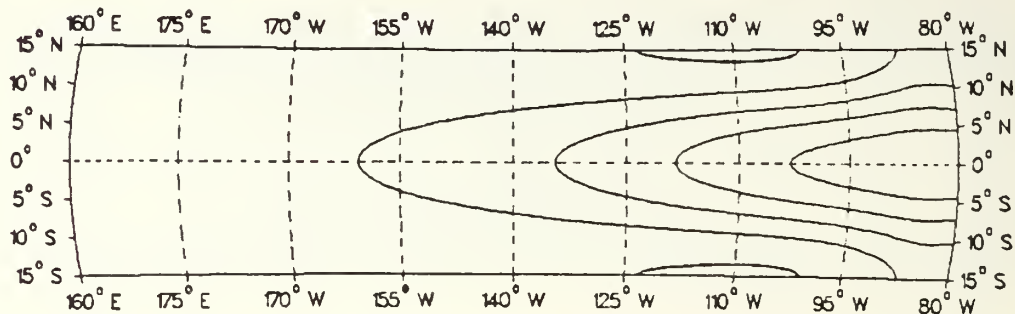


Figure 4.22 Case two, SST anomalies (deg C) for entire basin (day 350 and 400).

SST ANOMALY AT DAY 450  
CONTOUR INTERVAL = 0.0010



SST ANOMALY AT DAY 500  
CONTOUR INTERVAL = 0.0005

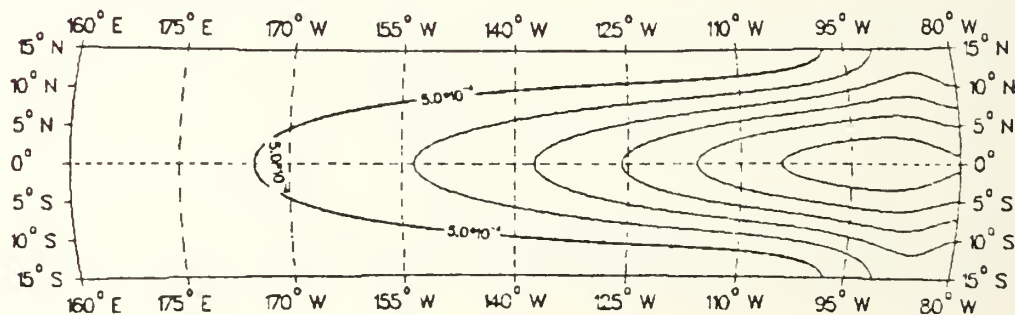


Figure 4.23 Case two, SST anomalies (deg C) for entire basin (day 450 and 500).

# SST ANOMALY AT EQUATOR

CONTOUR INTERVAL = 0.0010

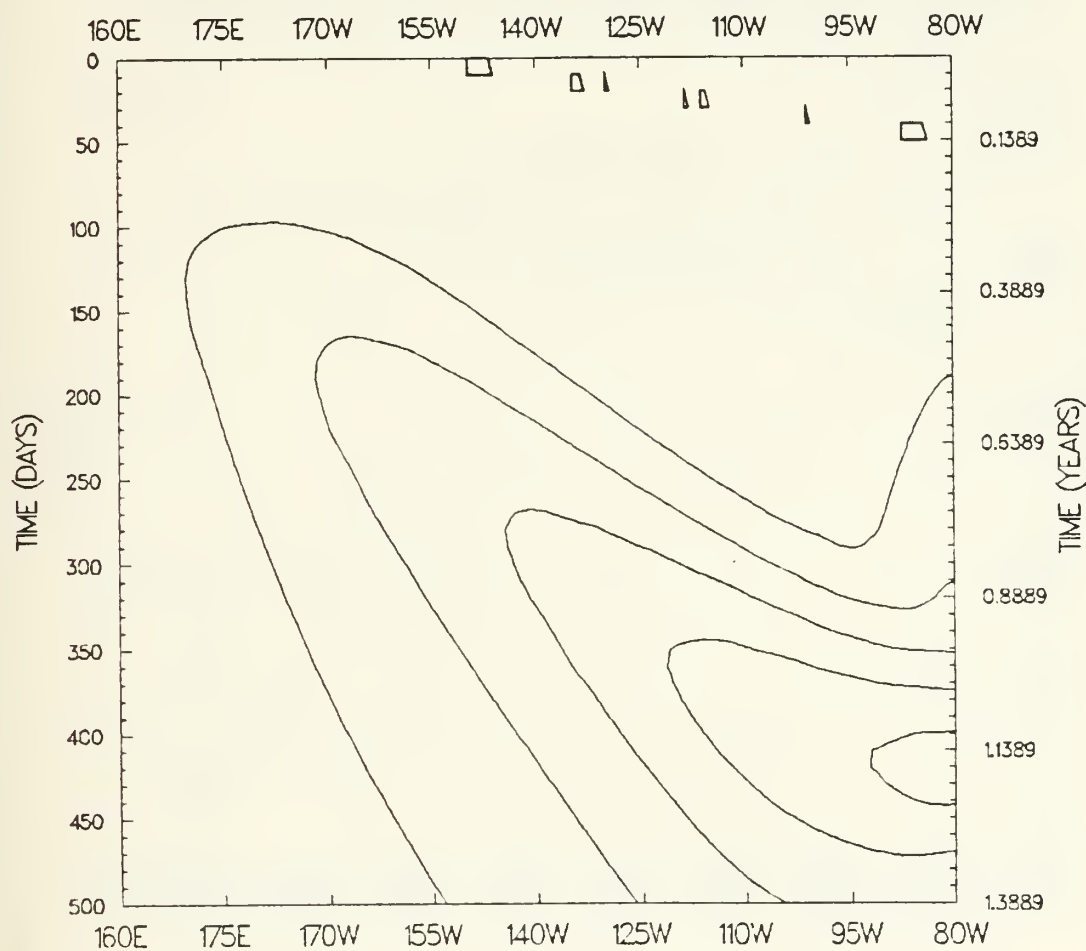


Figure 4.24 Case two, SST anomaly (deg C)  
time-longitude plot.

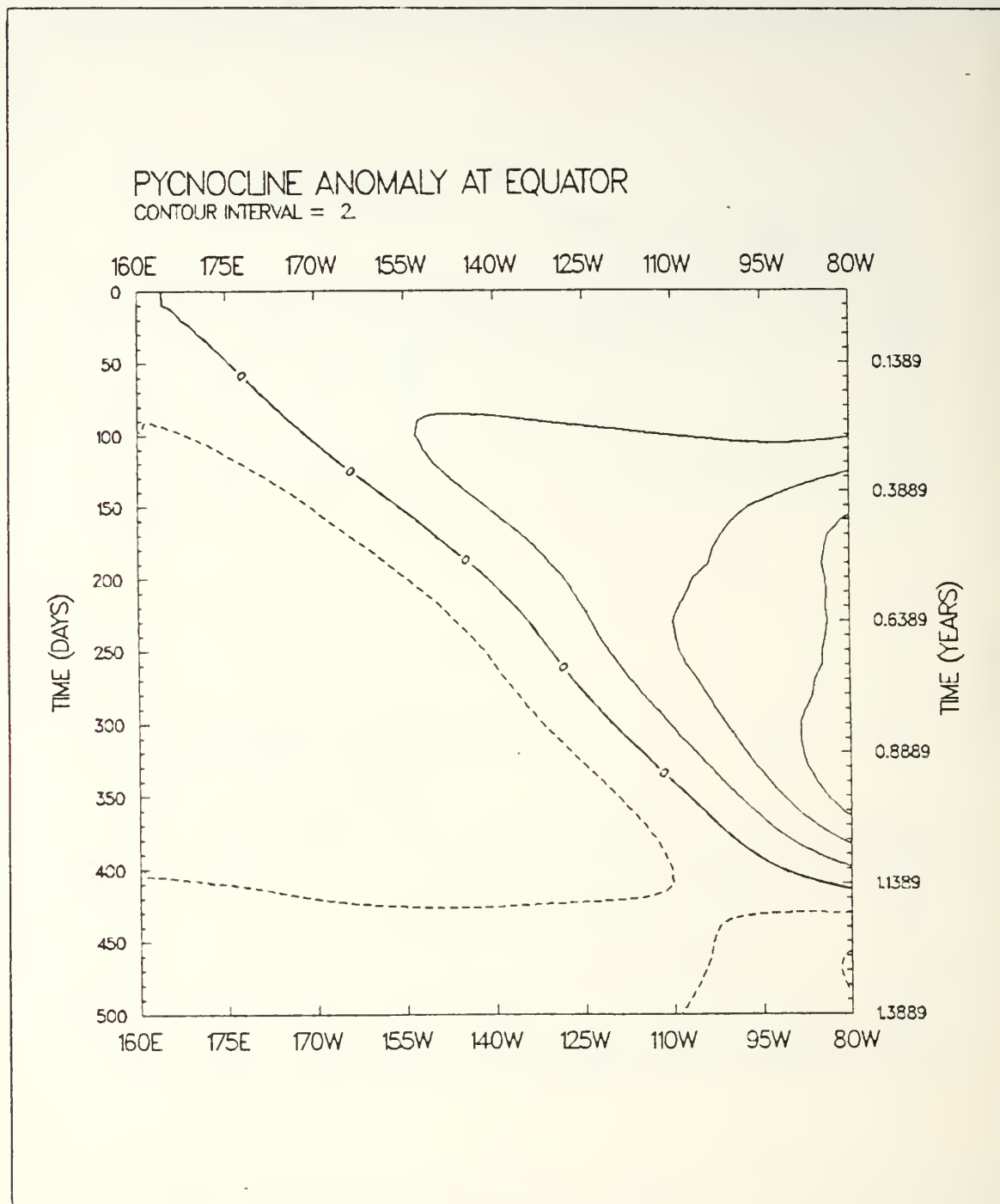


Figure 4.25 Case two, pycnocline depth anomaly (m)  
time- longitude plot.

# PYCNOCLINE ANOMALY AT EQUATOR

CONTOUR INTERVAL = 1.

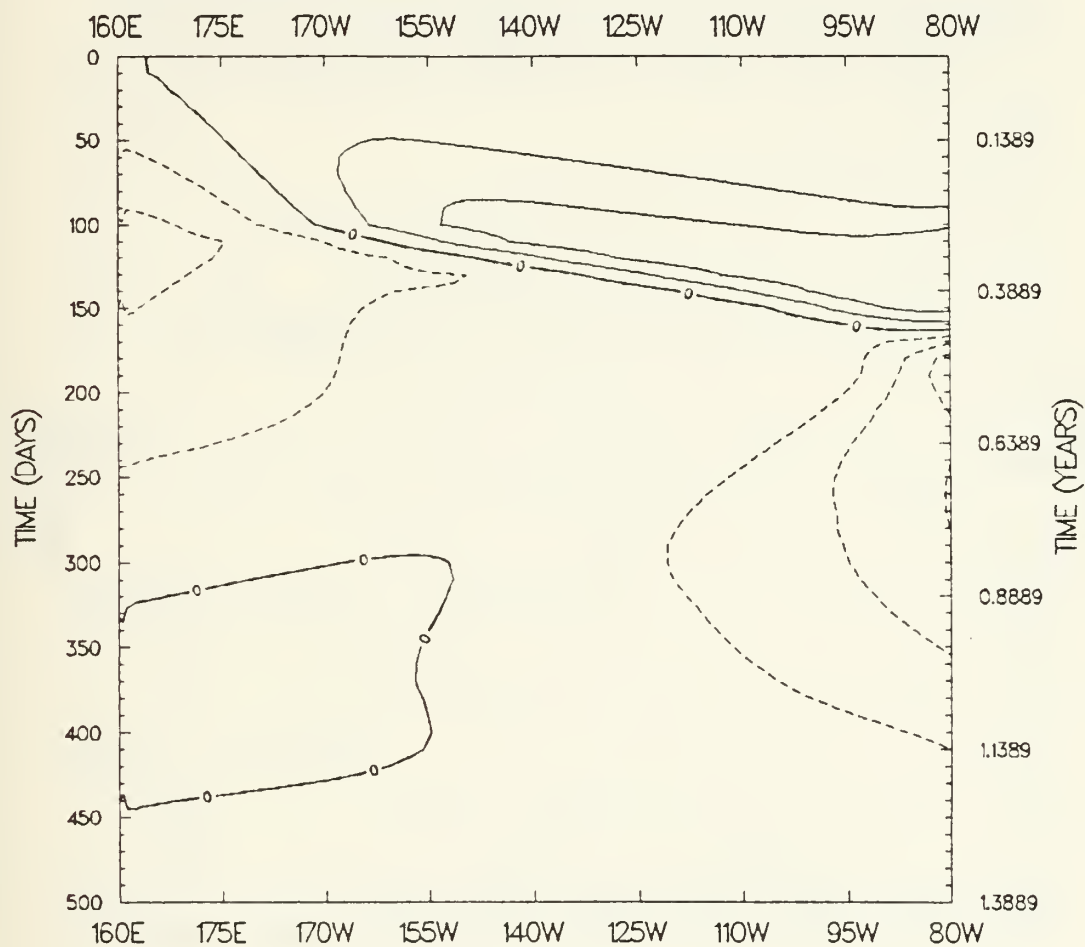


Figure 4.26 Case four, pycnocline depth anomaly (m)  
time- longitude plot.



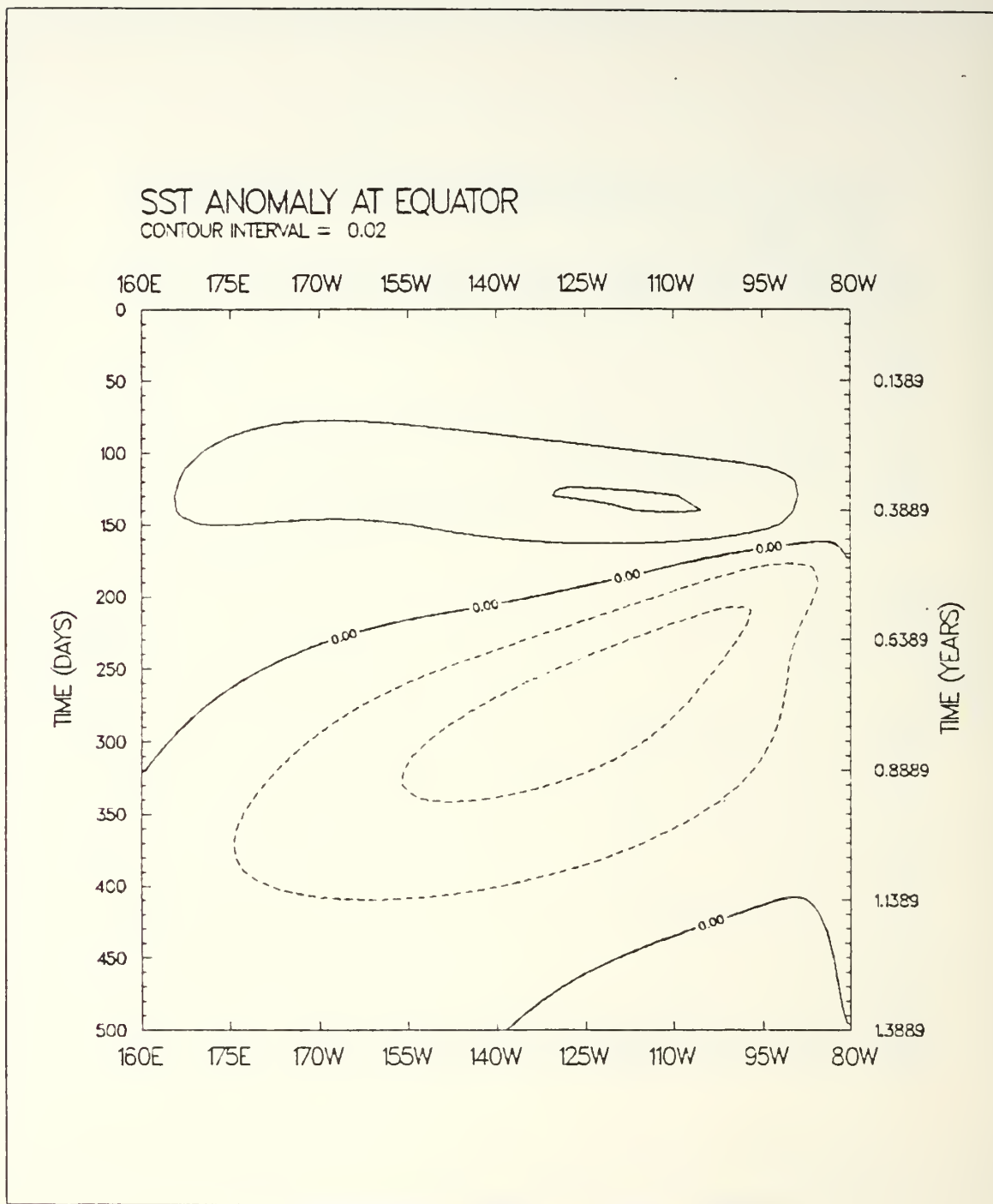


Figure 4.27 Case four, SST anomaly (deg C)  
time-longitude plot.

# PYCNOCLINE ANOMALY AT EQUATOR

CONTOUR INTERVAL = 2

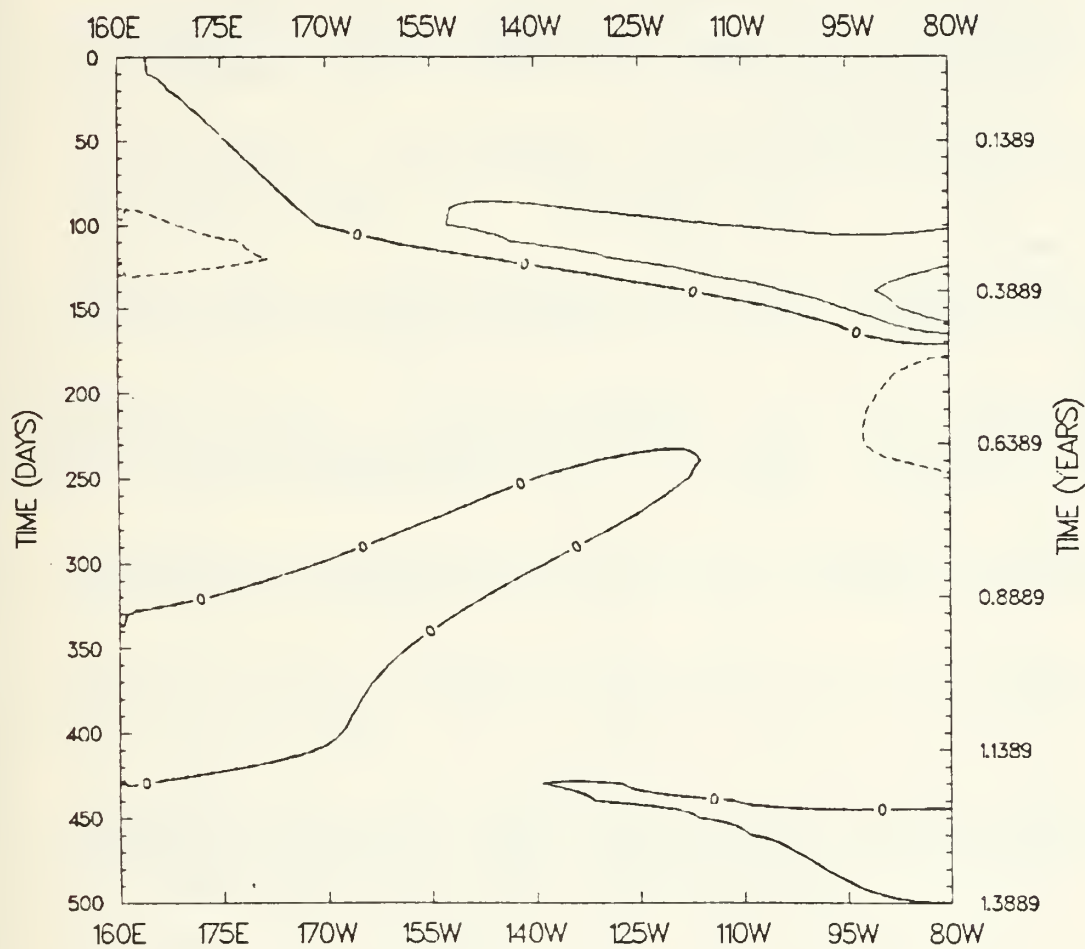


Figure 4.28 Case five, pycnocline depth anomaly (m)  
time- longitude plot.

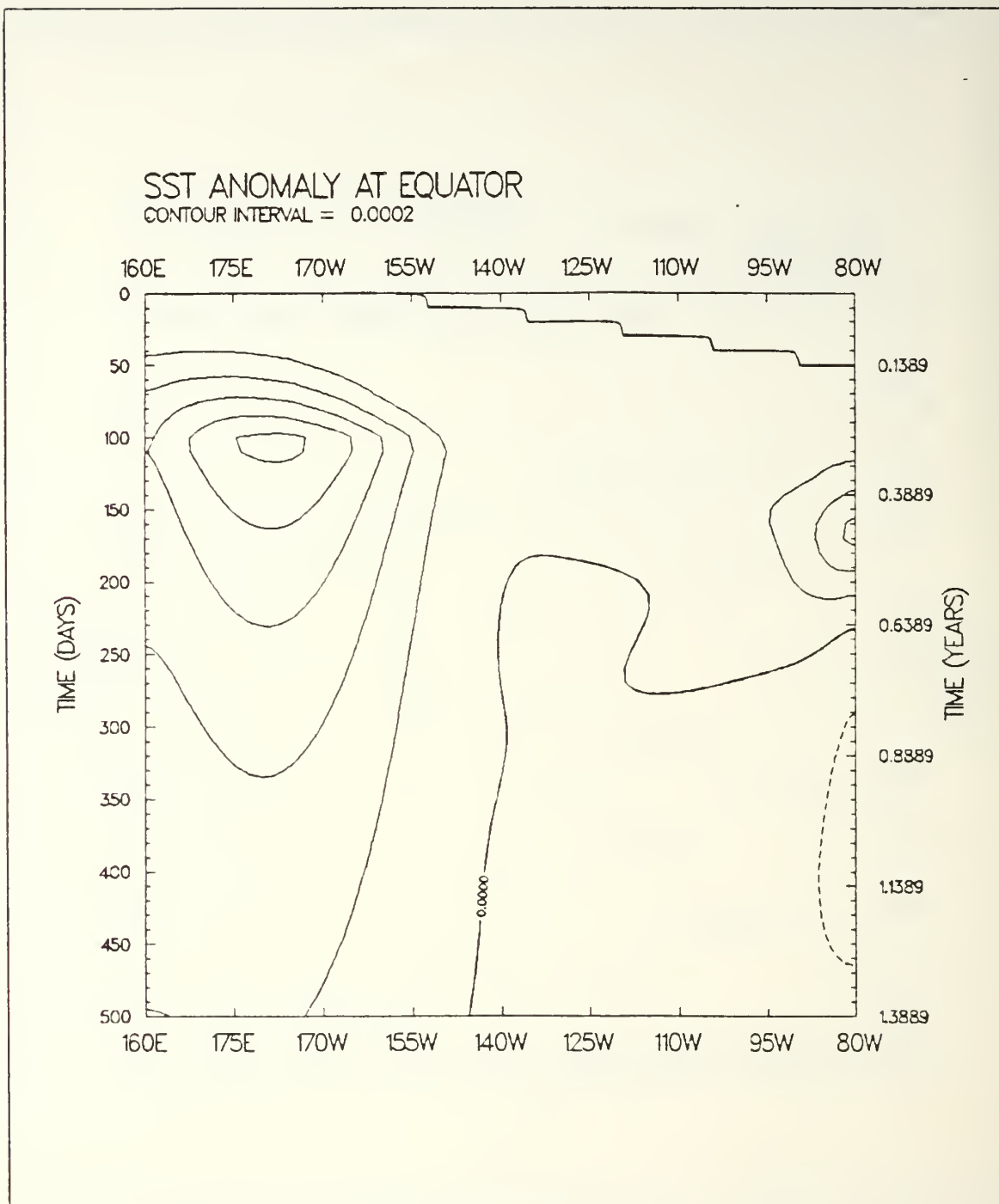


Figure 4.29 Case five, SST anomaly (deg C)  
time-longitude plot.

## LIST OF REFERENCES

1. Blundell, J.R. and Gill, A.E., "Equatorial Ocean Response to Wind Forcing," Ocean Modeling, v. 53, pp. 10-11, 1983.
2. Busalacchi, A.J. and O'Brien, J.J., "Interannual Variability of the Equatorial Pacific in the 1960's," J. Geophys. Res., v. 86, pp. 10,901-10,907, 1981.
3. Busalacchi, A.J., Takuchi, K. and O'Brien, J.J., "Interannual Variability of the Equatorial Pacific-Revisited," J. Geophys. Res., v. 88, pp. 7551-7562, 1983.
4. Gill, A.E., "Some Simple Solutions for Heat Induced Tropical Circulations," Quart. J. Roy. Meteor. Soc., v. 106, pp. 447-462, 1980.
5. Gill, A.E., "An Estimation of Sea-Level and Surface-Current Anomalies During the 1972 El Nino and Consequent Thermal Effects," J. Phys. Oceanogr., v. 13, pp. 586-606, 1983.
6. Gill, A.E., and Rasmusson, E.M., "The 1982-83 Climate Anomaly in the Equatorial Pacific," Nature, v. 306, pp. 229-234, 1983.
7. Hanson, H.P., "Equatorial Waves in the Presence of Sea-Air Heat Exchange," J. Phys. Oceanogr., v. 13, pp. 1170-1178, 1983.
8. Harrison, D.E. and Schopf, P.S., "Kelvin-Wave-Induced Anomalous Advection, and the Onset of Surface Warming in El Nino Events," Mon. Wea. Rev., v. 112, pp. 923-933, 1984.
9. Hurlburt, H.E., Kindle, J.C., and O'Brien, J.J., "A Numerical Simulation of the Onset of El Nino," J. Phys. Oceanogr., v. 6, pp. 621-631, 1976.
10. Kraus, E.B., and Turner, J.S., "A One-Dimensional Model of the Seasonal Thermocline: II. The General Theory and its Consequences," Tellus, v. 19, pp. 98-106, 1967.
11. Lau, K.M., "Oscillations in a Simple Equatorial Climate System," J. Atmos. Sci., v. 38, pp. 248-261, 1981.

12. McCreary, J., "Eastern Tropical Ocean Response to Changing Wind Systems: With Application to El Nino," J. Phys. Oceanogr., v. 6, pp. 632-645, 1976.
13. McCreary, J.P., "A Model of Tropical Ocean-Atmosphere Interaction," Mon. Wea. Rev., v. 111, pp. 370-387, 1983.
14. Niiler, P. and Kraus, E.B., Modeling and Prediction of the Upper Layers of the Ocean, pp. 143-172, Pergamon Press, 1977.
15. Niiler, P.P., Tropic Heat - A Study of the Tropical Pacific Upper Ocean Heat, Mass and Momentum Budgets, pp. 30, Corvallis, Oregon, 1982.
16. Philander, S.G.H., "On Los Ninos," TO-AN, v. 21, pp. 17-19, 1983.
17. Rasmusson, E.M., "Meteorological Aspects of El Nino/Southern Oscillation," Fifteenth Technical Conference on Hurricane and Tropical Cyclones, American Meteorological Society, 1984.
18. Rennick, M.A., "Atmosphere-Ocean Coupling During a Warm Event in the Equatorial Pacific," Prox. 16th International Liege Colloquium on Ocean Hydrodynamics, (in press), 1985.
19. Rennick, M.A., and Haney, R.L., "Stable and Unstable Air-Sea Interactions in the Equatorial Region," J. Atmos. Sci., (in revision), 1985.
20. Schopf, P.S., "On Equatorial Waves and El Nino II: Effects of Air-Sea Thermal Coupling," J. Phys. Oceanogr., v. 13, pp. 1878-1893, 1983.
21. Stage, S.A., and Businger, J.A., "A Model for Entrainment Into a Cloud-Topped Marine Boundary Layer. Part I: Development of a Model and Application to a Cold Air Outbreak Episode," J. Atmos. Sci., v. 38, pp. 2213-2229, 1981.
22. U. of Hawaii, Report HIG-77-13, The Southern Oscillation - Patterns and Mechanisms of the Teleconnections and the Persistence, pp. 107, by P.B.Wright, 1977.
23. Weare, B.C. and Strub, P.T., Marine Climate Atlas of the Tropical Pacific Ocean. Contributions in Atmospheric Science No. 20, pp. 147, University of California, Davis, 1980.
24. Weare, B.C., Strub, P.T., and Samuel, M.D., "Annual Mean Surface Heat Fluxes in the Tropical Pacific Ocean," J. Phys. Oceanogr., v. 11, pp. 705-717, 1981.



25. Wyrтки, K., "An Estimate of Equatorial Upwelling in  
the Pacific," J. Phys. Oceanogr., v. 11, pp.  
1205-1214, 1981.

# INITIAL DISTRIBUTION LIST

	No.	Copies
1. Defense Technical Information Center Cameron Station Alexandria, VA 22304-6145	2	
2. Library, Code 0142 Naval Postgraduate School Monterey, CA 93943-5100	2	
3. Chairman, Code 63Rd Department of Meteorology Naval Postgraduate School Monterey, CA 93943-5100	1	
4. Professor M.A. Rennick, Code 63Rn Department of Meteorology Naval Postgraduate School Monterey, CA 93943-5100	1	
5. Professor R.L. Haney, Code 63Hy Department of Meteorology Naval Postgraduate School Monterey, CA 93943-5100	2	
6. Professor R.W. Garwood, Code 68Gd Department of Oceanography Naval Postgraduate School Monterey, CA 93943-5100	1	
7. Commanding Officer Naval Ocean Research and Development Activity NSTL Station Bay St. Louis, MS 39522	1	
8. Commanding Officer Naval Environmental Prediction Research Facility Monterey, CA 93940	1	
9. Chairman, Code 68Mr Department of Meteorology Naval Postgraduate School Monterey, CA 93943-5100	1	
9. J.J. Waterreus, Lt. USN. 1100 Elm Avenue Provo, Utah 84604	1	
10. Director Naval Oceanography Division Naval Observatory 34th and Massachusetts Avenue Washington, DC 20390	1	
11. Commanding Officer Fleet Numerical Oceanography Center Monterey, Ca 93940	1	
12. Commanding Officer Naval Ocean Research and Development	1	

	Activity NSTL Station Bay St. Louis, MS 39522	
13.	Chairman, Oceanography Department U.S. Naval Academy Annapolis, MD 21402	1
14.	Chief of Naval Research 800 N. Quincy Street Arlington, Va 22217	1
15.	Office of Naval Research (Code 420) Naval Research and Development Activity 800 N. Quincy Street Arlington, Va 22217	1
16.	Scientific Liaison Office Office of Naval Research Scripps Institution of Oceanography La Jolla, CA 92037	1
17.	Library Scripps Institution of Oceanography P.O. Box 2367 La Jolla, CA 92037	1
18.	Library Department of Oceanography University of Washington Seattle, WA 98105	1
19.	Library CICESE P.O. Box 4803 San Ysidro, CA 92073	1
20.	Library School of Oceanography Oregon State University Corvallis, OR 97331	1
21.	Commander Oceanographic Systems Pacific Box 1390 Pearl Harbor, HI 96860	1
22.	Chief, Ocean Services Division National Oceanic and Atmospheric Administration 8060 Thirteenth Street Silver Springs, MD 20910	1









215376

Thesis

W229987

Waterreus

c.1

A model study of  
the equatorial ocean  
surface temperature  
response to wind forcing  
during El Nino.





DUDLEY KNOX LIBRARY



3 2768 00018019 4